University of Melbourne School of Physics

Masters Thesis 2012

Analysis of Neutrino Mass Effective Operators and Testing their Signatures at the Large Hadron Collider

Nicholas Rodd

Supervised by Professor Ray Volkas and
Professor Elisabetta Barberio

Abstract

Effective operators have emerged as a powerful framework for analysing the landscape of neutrino mass models. In this thesis we expound three contributions to the framework: 1. Highlight the challenges associated with generating consistent models from 11 dimensional operators; 2. Outline several constraints on the general UV completion of these operators; and 3. Demonstrate how to exactly evaluate two loop integrals in the zero momentum rest frame. Finally we verify the importance of using data from the Large Hadron Collider to set constraints on neutrino mass models. We do this through a presentation of the ATLAS same sign dilepton analysis, which is then used to set limits on the well known Zee-Babu Model.

Contents

Acknowledgements

Most importantly I have to thank Ray, Elisabetta and Archil who each supervised different parts of my research. It is only through their patience and insights that this work has been able to be completed. Similarly I would like to thank Kenji Hamano for the immense support he provided me in our collaboration with the same sign dilepton analysis. I must also thank Bruce McKellar for useful discussions on the evaluation of two loop integrals. Finally to all the official and unofficial former residents of room 302, thanks for always keeping a smile on my face.

Statement of Contributions

Section 1, 2 and 3, as well as Appendix B and C contain the author's own work. Appendix A is a summary of existing work. Section 4 is the work of a collaboration of which the author was a part. Various aspects of this work have been submitted for publication in three papers [41, 42, 52].

1 Introduction

1.1 The Problem of Neutrino Masses

As the Large Hadron Collider closes in on what appears to be a Standard Model Higgs boson, the question of how the mass of the neutrino can be added to the canonical picture of mass generation is more pertinent than ever. For even though the Higgs would complete the Standard Model (SM) and give credence to the concepts of electroweak symmetry breaking and fundamental mass generation through interaction with a background field, the model cannot be an exhaustive picture of reality. There are many well documented shortcomings, such as its incompatibility with gravity, the hierarchy problem, the lack of a baryogenesis mechanism and the absence of a dark matter candidate. Nevertheless neutrino masses represent a much more straightforward failing of the SM: it predicts neutrinos to be massless, which is in stark contradiction with the evidence that has been emerging since 1998 [1, 2, 3] that neutrinos have a small but non-zero mass. In essence the experiments have observed neutrino oscillations, which occur when a neutrino changes its flavour between where it is created and detected. This is a phenomenon only possible for massive particles. Theorists had contemplated the different ways the SM could be augmented to incorporate neutrino masses even before this discovery and coming up with so called neutrino mass models has become a small industry since then. Generically these models predict new particles that couple to SM fields. Such particles can be searched for at colliders using the data emerging from the Large Hadron Collider (LHC), which is complementary to the constraints from oscillation data or rare processes like neutrinoless double beta decay ($\beta\beta0\nu$).

In order to stay on top of all of these models, Babu and Leung have introduced the concept of effective operators as a structure existing above individual models and a way to approach the generation of such models systematically [4]. This concept has been built upon by de Gouvêa and Jenkins [5] and most recently Volkas and Angel [6]. The focus of this thesis will be on contributing to the effective operator literature and more specifically looking into how data emerging from the LHC can be exploited to constrain such models. The thesis will be structured as follows. In this section we provide a review of the effective operator concept. In section 2 we describe an incomplete attempt to rule out higher dimensional operators and outline several challenges with creating consistent models from such operators. In section 3 we document a number of constraints on the general UV completion of effective operators. In section 4 we describe how one neutrino mass model, the Zee-Babu Model, was tested using 7 TeV ATLAS data. Appendix A and B contain a summary of how to calculate two loop integrals. Finally appendix C provides a short summary of a side project completed on time symmetric Quantum Field Theory (QFT) and Hawking Radiation.

1.2 Introduction to Neutrino Mass Models

1.2.1 Technical Aspects of Mass Generation

Before describing how mass models can be categorised into effective operators, it is worth reviewing the problem in a more technical setting. As outlined above the existence of neutrino masses presents a problem for the SM that is simple enough to state: neutrino mass exists and it is small.

Accordingly the task for any mass model is to provide a mechanism for mass generation and furthermore a natural explanation for why the mass is so small.

This second point is worth stressing. Naively one might not think there is that much of a problem. Experimental evidence suggests the mass of the heaviest neutrino can be at most of order 1 eV, which is around six orders of magnitude lighter than the next smallest fermion, the electron at 0.511 MeV. But the top quark at roughly 174 GeV is almost six orders of magnitude larger again and we generally put the difference between the electron and top down to a difference in couplings to the Higgs; why can the same not be true for neutrinos? The neutrino case is different for at least two reasons. Firstly it is not just one neutrino which is that much lighter, but all three. While this may be a coincidence, it would be preferable if our models could explain it. Secondly there is a technical reason why it is artificial to write down a mass term for the neutrinos in the same way we do for the other fermions. To understand this we have to consider the different ways fermions can be given masses.

Lorentz invariance allows chiral fermions to acquire mass in two ways. Firstly we can write a Dirac mass term, which for a fermion ψ is usually denoted by $m\overline{\psi_L}\psi_R$. This is how fermions acquire mass in the SM. For example, the electron acquires mass through the term $H\overline{L_L}e_R$, which gives rise to a Dirac mass term once the Higgs field H acquires a vacuum expectation value (VEV). Such a mass is not possible for the neutrino in the SM as the neutrino only enters as ν_L in the lepton doublet L - there is no ν_R to complete a Dirac mass term. The second possibility is a Majorana mass, which is written as $m\overline{\psi_L^c}\psi_L$. Note $\psi^c \equiv C\overline{\psi}^T$ where C is the charge conjugation operator. Again in the SM this is not allowed as such a term for ν_L has to be written using L and would violate hypercharge. Indeed the only way such a term would not violate hypercharge is if $Y(\psi) = 0$. In general a Majorana mass term will violate any $U(1)$ quantum numbers carried by ψ and this implies that such a term for the neutrino must violate lepton number by exactly two units.

The failure of either mechanism to work for the neutrino in the SM shows us why it predicts no neutrino mass at the first order of perturbation theory or tree level. The reason why the SM predicts a zero neutrino mass at all orders is because it exactly conserves lepton number; the black box theorem [7, 8] proves that models that violate lepton number induce a neutrino mass at some order and vice versa.

1.2.2 Type I Seesaw Model

We have seen above why there cannot be a neutrino mass in the SM. Nevertheless it has also given us insight into how we might go about modifying the model to include it. If we wanted a Dirac mass term for the neutrino then we need to introduce a right handed neutrino ν_R and furthermore in order for the mass term to be gauge invariant it is not hard to see that it must transform under the SM gauge group $SU(3) \otimes SU(2)_L \otimes U(1)_Y$ as $\nu_R \sim (1, 1, 0)$. The surprising feature of such a particle is that its transformations are such as to allow a gauge invariant Majorana mass term to be written down for ν_R. The golden rule of model building is that all gauge invariant terms should be included unless forbidden by a symmetry. Of course adding such a term would break lepton number symmetry, but as this only arises as an accidental symmetry in the SM it does not seem unreasonable to break it in favour of adding an additional gauge invariant term. Accordingly as

soon as we try to give the neutrino a Dirac mass we are almost compelled to give ν_R a Majorana mass. This is the technical difficulty alluded to above - unless one insists on maintaining lepton number as a symmetry of the SM, there is no way to simply give the neutrino just a Dirac mass like the other fermions.

Adding both terms above leads to the following addition to the SM Lagrangian

$$\mathcal{L} \supset \left(\lambda_\nu H^c \overline{L} \nu_R + h.c.\right) + M \overline{\nu_R^c} \nu_R, \tag{1.1}$$

where λ_ν is the Yukawa coupling for the neutrino and M is the Majorana mass of ν_R. Interestingly M is not protected by a gauge symmetry (there is nothing like a Higgs coupling that would suggest it should be related to the electroweak scale) and so there is no reason it cannot be much larger than other fermion masses.

What we have just written down is the Lagrangian of the Type I Seesaw Model [9, 10, 11, 12], which is seen by many as the leading candidate for neutrino masses. To see where it gets its name, observe that after expanding around the Higgs VEV v and setting $m = \lambda_\nu v$ equation (1.1) gives the following mass matrix:

$$\frac{1}{2} \begin{pmatrix} \overline{\nu_L} & \overline{\nu_R^c} \end{pmatrix} \begin{pmatrix} 0 & m \\ m & M \end{pmatrix} \begin{pmatrix} \nu_L^c \\ \nu_R \end{pmatrix}, \tag{1.2}$$

which when diagonalised yields two mass eigenvalues, m^2/M and M. Increasing the value of heavier mass decreases the mass of the lighter one, which is where the model gets its name. As noted M can be huge and thus this model provides a natural explanation for the small observed neutrino mass. It owes its popularity to both its simplicity and the fact it is the first route one would consider when trying to give the neutrino a mass. It also appears as a natural consequence of many extensions of the SM such as the left-right symmetric model [13, 14, 15, 16] or $SO(10)$ GUT theories [17]. The downside is that a fit to current data requires $M \sim 10^{11}$ TeV - a mass well beyond the reach of foreseeable experiments, making this model essentially impossible to test directly.

1.2.3 From Seesaws to Effective Operators

The Type I Seesaw is only the starting point of the landscape of neutrino mass models. In a somewhat similar manner, augmenting the SM with a scalar triplet $\Phi \sim (1, 3, 2)$ or a fermion triplet $f_R \sim (1, 3, 0)$ instead of ν_R, a seesaw type mechanism can again be induced yielding what is known as the Type II [18, 19, 20, 21, 22, 23] and III [24] Seesaw Models respectively. These may not be as compelling as the Type I, but they predict new physics at lower energy scales and are in fact both being searched for directly at the LHC. Rather than going through the details as we did for the Type I, a convenient way to visualise what is going on here is to draw the Feynman diagram that generates the Majorana neutrino mass in these models. This has been done in Figure 1.1.

As soon as these diagrams have been written down we can see there is a manifest similarity between all three models, namely the $LLHH$ structure which has been highlighted. The only difference between them is the new particles that connect the external structure - more specifically they differ only in their ultraviolet (UV) completion. Given that ν_R, Φ and f_R have not been

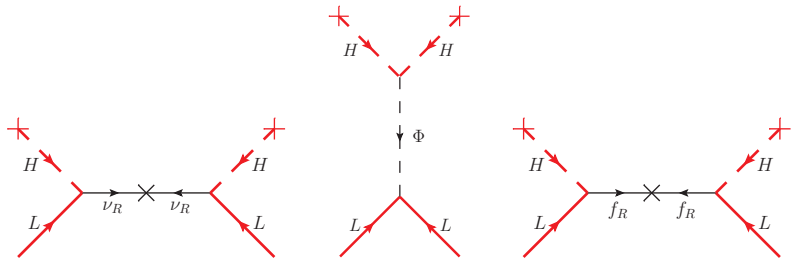

Figure 1.1: Type I (left), II (centre) and III (right) Seesaws with common structure highlighted.

experimentally observed it is reasonable to posit that if they do exist they will have masses well above L or H. Accordingly we can integrate out the new physics, which leads to the generic structure seen in Figure 1.2.

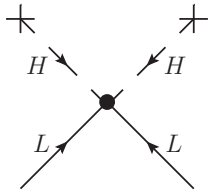

Figure 1.2: A common thread between the Seesaw Models - $\mathcal{O}_1$.

This non-renormalizable vertex is referred to as $\mathcal{O}_1$ in the literature, as it is the first effective operator in the language of Babu and Leung's paper. It is usually written as

$$\mathcal{O}_1 = L^i L^j H^k H^l \epsilon_{ik} \epsilon_{jl}, \tag{1.3}$$

where Roman letters are used to denote $SU(2)$ indices. Written like this it is clear $\mathcal{O}_1$ is just the Weinberg operator [25]. The fundamental idea is that $\mathcal{O}_1$ is an abstraction that sits on top of the Seesaw Models. It contains the key details for neutrino mass generation - specifically it breaks lepton number by two units - but does so at the cost of knowing the specific phenomenologies of individual models. Not all models will be able to be integrated back to $\mathcal{O}_1$. In fact the vast majority of neutrino mass models are quite different from the Seesaw Models seen above. It can be shown that these are the only possible tree level models; all remaining models induce a Majorana mass for the neutrino at one or more loops. Such models rely on the loop suppression to explain the smallness of the neutrino mass rather than a seesaw type mechanism.

It should be noted that the concept of effective operators is not a new one and is in fact equivalent to the notion of effective theories, the classic example being Fermi's four fermion model. Figure 1.3 below hopefully clarifies the concept of effective operators - the idea is that at energies well below M_W the propagator can be integrated out and the physics can be well described by the non-renormalizable vertex $\overline{u}d\overline{\nu}e$.

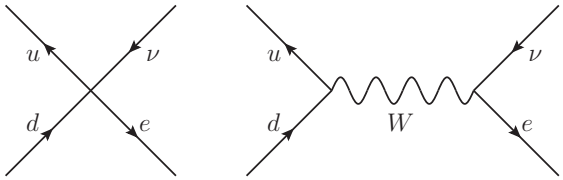

Figure 1.3: Fermi's four fermion operator (left) and its UV completion (right).

1.3 Effective Operators as a Systematic Approach to Neutrino Mass

The true utility of effective operators, however, is that they can be used in the taxonomy of neutrino mass models. This was the insight in Babu and Leung's original paper: effective operators rather than individual models should be the starting point. The reason is that they showed there is actually only a finite number of neutrino mass effective operators. This allows one to systematically work through the different operators and consider which are constrained or ruled out by experimental data. In this way, even if the Type I Seesaw is the model nature chose for neutrino mass, it can be given substantial indirect evidence if the alternatives can be ruled out.

The original list contains 75 different operators, all of which can be generated from a simple recipe. To begin with the operator cannot break baryon number - it must have $\Delta B = 0$. If it did it would give rise to models that contain proton decay or other processes that are highly constrained by experimental data. These constraints would force the couplings to be so small that the model could not generate a neutrino mass consistent with the atmospheric neutrino oscillation data, which shows at least one neutrino must have a mass greater than 0.05 eV [2]. In addition, to generate a Majorana neutrino mass the operator must have $\Delta L = 2$ (break lepton number by two units). For example in $\mathcal{O}_1$ this is done by LL. Then one can add additional groups of SM fields with $\Delta L = \Delta B = 0$ as long as the operator stays below mass dimension 13.

This final point on the dimension was the crucial step in Babu and Leung's paper as it implies the list is finite and it is worth summarising their argument. In QFT all Lagrangian terms must have a mass dimension of four on dimensional grounds. Furthermore it can be shown that the field content of renormalizable terms must have dimension of at most four. This is not true of the effective operators because they are not a full description of what is going on - the high energy degrees of freedom have been integrated out. Nevertheless the high energy effects cannot be completely disregarded as they suppress the couplings of the effective interactions. For example Fermi's four fermion theory has a 6D interaction and to get this back to a 4D Lagrangian term the coupling constant must have dimension -2. Indeed we know that $G_F \propto m_W^{-2}$. More generally an nD effective operator will be suppressed by (n-4) dimensions of the scale of the physics that has been integrated out. In addition it is hard to hide the new degrees of freedom from neutrino mass models as they generically couple to SM fermions, especially leptons. Accordingly their non-observation at colliders implies they must be heavier than about 100 GeV. Babu and Leung showed that for 13D operators, the $(100\text{GeV})^{-9}$ suppression prevents these models from being able to predict a 0.05 eV neutrino mass as required from atmospheric data. In this way they were able to show the 75

operators outlined in their paper were the only ones possible. The list contains 1 5D ($\mathcal{O}_1$), 7 4D, 15 9D and 52 11D operators, with all except for $\mathcal{O}_1$ containing 4 or 6 fermions.

Subsequent to this de Gouvêa and Jenkins provided an order of magnitude approximation of the best way to experimentally test different operators, for example through looking for new particles at the LHC or alternatively through rare processes like $\beta\beta0\nu$ and lepton number violating decays such as $\mu \to e\gamma$. One of the results they provided that we will draw on in this thesis is that for each operator they determined an approximate scale of the new physics involved. To do this they approximated the neutrino mass allowed by an operator in the following way: include a loop suppression of $(16\pi^2)^{-n}$, where n is the smallest number of loops the operator can be closed off in; include any SM masses the operator structure would introduce; and finally divide by the scale of new physics, Λ, required by the operator (e.g. 5D requires 5-4=Λ^1, or 11D requires 11-4=Λ^7). Then they set this formula equal to the atmospheric limit and extracted a value for Λ. In their paper they also showed that a number of the operators are already highly disfavoured by existing data.

The next development came in the recent work of Volkas and Angel. There they provided a general procedure for how to generate one and two loop models from a given operator. Note that although it has not been rigorously proven yet, it is generally assumed that three loop models would suppress the masses too greatly to fit the atmospheric limit. This work is crucial to the analysis of individual operators, as one can write down all models a given operator can give rise to and analyse their phenomenology in detail.

It would not be practical to fully outline their procedure here - it should be clear from the example of $\mathcal{O}_1$ above that a single operator can give rise to many models. In short they provide an exhaustive list of all possible UV completions for four and six fermion operators. One of their most interesting results is that they were able to show that 25 operators cannot be closed in two loops or less. As stated above three loops is highly disfavoured and as such so are these operators. The operators this rules out are 15-20, 34-38, 43, 50, 52-60, 65, 70 and 75. Interestingly de Gouvêa and Jenkins' analysis suggests an even larger class of operators would be ruled out this way. This discrepancy is addressed in section 2.

As section 2 and 3 of this thesis will draw extensively on their method for opening up the six fermion operators, a brief outline is provided here. To begin with the starting point is a vertex with six fermions and potentially several Higgs. The next step is the UV completion, for which there are several options. The simplest of these is to just use scalars in the UV completion as seen on the left of Figure 1.4.

Note that the direction of the scalars in the diagram is arbitrary. The next step is to close off the external fermions in a way that provides a valid Majorana neutrino mass diagram - which has the generic structure of two external neutrinos. As discussed by Volkas and Angel, this cannot be done by putting two L fields at the same vertex as this would induce the Type II Seesaw Model (compare Figure 1.1 centre) and as this is a tree level process it would dominate over the two loop. Accordingly the L fields must be at different vertices and then the unique closure is shown on the right of Figure 1.4.

There are a few points worth commenting on in this diagram. To begin with the reason for the external $\overline{L^c}L$ rather than LL is that the matrix structure of the latter term does not make sense; it is simply a convenient shorthand. Despite this, sometimes in the literature these diagrams are

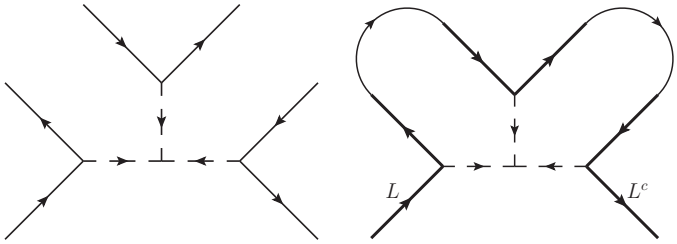

Figure 1.4: Scalar UV completion (left) and closure (right) of six fermion operators.

depicted with two L fields, see e.g. Figure 1.1, but the two are interchangeable. Secondly the way the fermion lines have been closed must be appreciated as a shorthand. There are two possible ways of closing off the SM fields from the original operator: 1. Connect a field to its adjoint, e.g. a $\overline{u}u$ coupling; or 2. Connect fields through a Higgs coupling, e.g. $\overline{Q}dH$, where the Higgs is then replaced by its VEV. In Figure 1.4 only the former has been drawn, but this is a shorthand for either possibility.

The only other possible modification of this scalar UV completion is to use Higgs fields from the operator to avoid inducing the Type II Seesaw when the L fields are at the same vertex. An example of this is shown below.

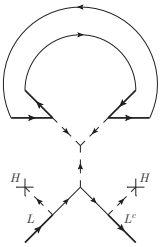

Figure 1.5: Second scalar UV completion.

The other way to UV complete six fermion operators is with an exotic fermion. There are five different ways such diagrams can be closed as shown in Figure 1.6 where Volkas and Angel's naming procedure was used. Diagram C and D2 may initially look somewhat different from the others, but this is because we have drawn them in a simpler, but topologically equivalent way to how they were drawn by Volkas and Angel.

This exhausts the different possibilities for diagrams from six fermion operators. There are some extra features that can be added by placing Higgs in various positions, as discussed by Volkas and Angel, but there are no extra diagrams. With all the ingredients in place we can now give a concrete example of how to move from an operator to a model. Consider the following operator:

$$\mathcal{O}_9 = L^i L^j L^k e^c L^l e^c \epsilon_{ij} \epsilon_{kl} \,, \tag{1.4}$$

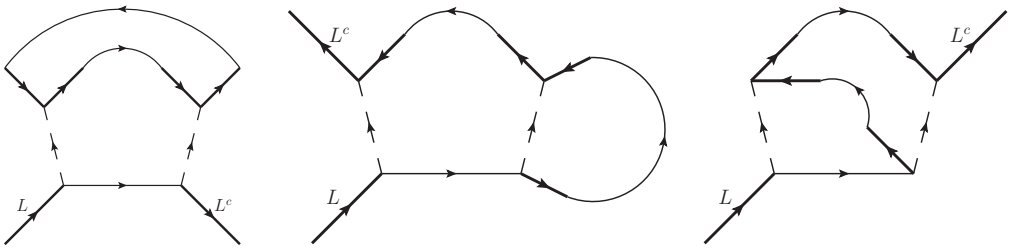

(a) Diagram A (left), B (centre) and C (right)

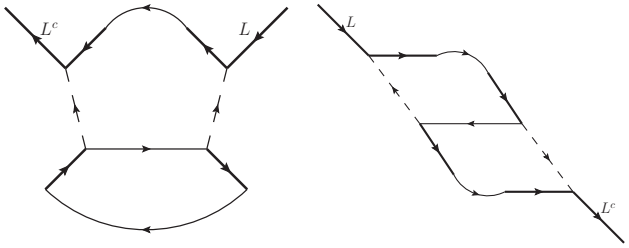

(b) Diagram D1 (left) and D2 (right)

Figure 1.6: Central Fermion UV completions.

this can be UV completed with scalars and then closed off using Higgs couplings as in Figure 1.7. The two loop model on the right is in fact the well known Zee-Babu Model (ZBM) that was discovered well before the effective operator analysis [26, 27]. This model will be used as a test case for how LHC data can be used to constrain such models in section 4.

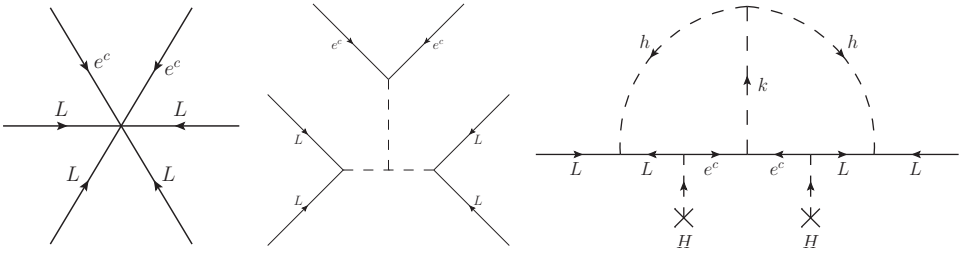

Figure 1.7: $\mathcal{O}_9$ (left), with one possible UV completion (centre) and the closed two loop model (right).

The real utility of Volkas and Angel's analysis is that they exhaust the possible UV completions and therefore it becomes possible to systematically write down all models from a given operator. Although the process looks relatively straightforward, in attempting to come up with two models based on 11D operators a number of unexpected complications arose, including a number of general constraints on their analysis. These constraints are detailed in section 3, but before looking at them we turn our attention to 11D effective operators.

2 Analysis of 11D Effective Operators

As discussed, Babu and Leung concluded that 13D operators generate neutrino mass models that are inconsistent with current experimental data. Nevertheless this conclusion was reached in 2001; improvements on precision data since then and especially the results now emerging from the LHC may mean that the same argument can be extended to exclude 11D operators. This would rule out a large class of operators and when combined with the removal of operators that Volkas and Angel observed cannot be closed in two loops or less, there would only be 14 remaining possible operators from which a Majorana neutrino mass model could emerge. This would make the class of effective operators small enough that it would become feasible to write down all minimal models that could generate neutrino mass and test them one by one.

In order to test this hypothesis we decided to construct models from two arbitrary 11D operators, $\mathcal{O}_{68_b}$ and $\mathcal{O}_{31_a}$, in the hope that we could see if they were ruled out by existing data and if so generalise such arguments to other 11D operators. What we ultimately found is that it is much harder than originally thought to construct consistent 11D models - such models generically induce a neutrino mass associated with a lower dimension operator, making it impossible to study the 11D structure in isolation. This last point will be clarified through the analysis of the two models below.

As an aside one of the main pieces of work involved in analysing these models was an exact evaluation of their mass matrices, which required an exact determination of their associated two loop integrals. The details of these calculations are lengthy and so have been relegated to appendices A and B. Traditionally neutrino mass models evaluate the mass matrix by assuming several hierarchies to simplify the calculation, for example $m_{new} \gg m_{SM}$, see e.g. [6]. Often there are also assumptions as to hierarchies within the new particle masses. But in order to test models using LHC data, it is important to understand the implications of the new masses being at the TeV scale, and then it becomes highly unrealistic to fit several hierarchies between these and $m_{top} = 174$ GeV for example. Accordingly to facilitate LHC testability these calculations were done without approximations.

2.1 A Model from $\mathcal{O}_{68_b}$

In this section we use Volkas and Angel's procedure to develop a model from $\mathcal{O}_{68_b}$. It was chosen as de Gouvêa and Jenkins suggest it has a low associated scale of new physics - around 100 TeV. This energy assumes couplings of order unity; more realistic couplings would require smaller masses. Naively this would suggest models from this operator could be significantly constrained through a non-observation of their particles at the LHC. Note that $\mathcal{O}_{68_b}$ was chosen rather than operators with lower orders of new physics that can be closed in two loops, such as $\mathcal{O}_{26_b}$, by accident. This arose as initially $\mathcal{O}_{68_a}$ was used, until it was realised the $\overline{(L^i)^c} L^j \epsilon_{ij}$ contraction makes it impossible to have two external neutrinos without introducing a gauge boson and thus an extra loop. The operator itself has the following form:

$$\mathcal{O}_{68_b} = L^i L^j Q^k d^c H^l Q^r d^c \overline{H_r} \epsilon_{ik} \epsilon_{jl}, \tag{2.1}$$

which as discussed is a shorthand for the full structure which can be viewed as:

$$\mathcal{O}_{68_b} = \left[\overline{(L^i)^c} Q^k \epsilon_{ik}\right] \left[\, \bar{d} L^j H^l \epsilon_{jl}\right] \left[\, \bar{d} Q^r \overline{H_r}\,\right], \tag{2.2}$$

where the $SU(2)$ structures have been grouped. Note that in making this rearrangement we made use of the identity $\overline{\psi}\chi^c = \overline{\chi}\psi^c$.

Now this is a six fermion operator, so it can be converted into a model using one of the UV completions discussed in the introduction. For this purpose diagram B (see Figure 1.6) was used. An interesting feature that was discovered in the process of coming up with this model was that the choices of which diagram to use and the placement of the Higgs were not entirely arbitrary. Certain choices will in fact lead to either invalid diagrams, a two loop that actually generates a mass at one loop or a model that fails for some other reason. These results are collected in section 3.

2.1.1 Overview of the Model

Using diagram B we generated the diagram seen in Figure 2.1. It is worth highlighting that this model has been chosen as just a general model coming from $\mathcal{O}_{68_b}$. It is not well motivated by, for example, grand unification or some new symmetry and as such there is no reason it should not look as ugly as it does.

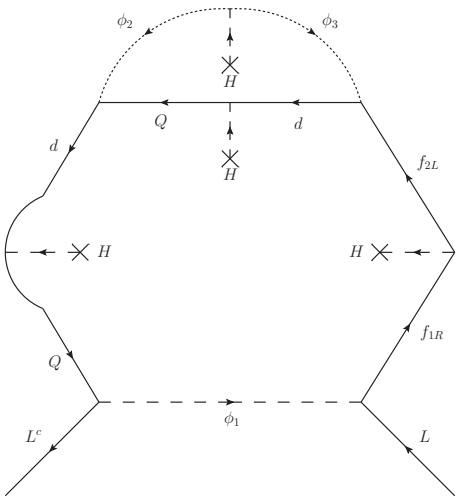

Figure 2.1: A model generated from $\mathcal{O}_{68_b}$.

As can be seen from the diagram, this model introduces five new fields with three scalars and two fermions. The quantum numbers of these new fields were determined using three principles: 1. Requiring gauge invariance at each vertex; 2. Ensuring the $SU(2)$ structure of equation (2.2) is maintained (e.g. that $\overline{H}$ and Q are '$SU(2)$ connected', which implies ϕ_2, ϕ_3 and f_{2L} cannot be weak isospin singlets); and 3. Choosing remaining freedoms so as to minimise the number of new couplings.

Point three is worth elaborating on. The first two principles are required for the validity of the model, but generally are not enough to entirely fix all quantum numbers. For example it is not hard to see that for this model these will not be able to determine whether ϕ_2 transforms under the singlet or adjoint representation of $SU(3)$. Nevertheless when determining the full Lagrangian for the model, one must consider all possible gauge invariant combinations of SM and new fields, which must be done systematically to ensure no terms are missed. Extra Lagrangian terms will complicate the model: they can lead to an induced one loop model that will dominate over the two loop, lead to new two loop models that will interfere with the original diagram or potentially introduce baryon number violation into the model. Accordingly whilst the most general model will contain such terms, in order to make the problem more tractable it is wise to restrict such terms with a judicious choice of the quantum numbers. Applying these principles to this model yields:

$$\begin{gathered}\phi_1 \sim (3,3,-2/3)\\ \phi_2 \sim (8,2,-1)\\ \phi_3 \sim (8,3,2)\\ f_{1R} \sim (3,4,-5/3)\\ f_{2L} \sim (3,3,-8/3)\end{gathered} \tag{2.3}$$

From here we can now write down the most general Lagrangian for this model, which will be made up of the following parts:

$$\mathcal{L} = \mathcal{L}^{SM} + \mathcal{L}^{new}_{kinetic} + \mathcal{L}^{new}_{\nu} + \mathcal{L}^{new}_{scalar} + \mathcal{L}^{new}_{extra} + \mathcal{L}^{new}_{fermion}, \tag{2.4}$$

where each term will be explained below. $\mathcal{L}^{SM}$ is the SM Lagrangian and $\mathcal{L}^{new}_{kinetic}$ contains the additional kinetic terms for the new fields (i.e. $(D_\mu\phi)^\dagger (D^\mu\phi)$ for scalars and $i\overline{f}\not{D}f$ for fermions). $\mathcal{L}^{new}_{\nu}$ contains the new terms required by the neutrino mass matrix in Figure 2.1 and is given by:

$$\mathcal{L}^{new}_{\nu} = g^1_{ab}\overline{L^c_a}Q_b\overline{\phi_1} + g^2_{cd}\overline{d_c}Q_d\phi_2 + h^1_e\overline{d_e}f_{2L}\phi_3 + h^2_f\overline{f_{1R}}L_f\phi_1 + \lambda\overline{f_{2L}}f_{1R}\overline{H} + \mu_{23}\overline{\phi_2\phi_3}H + h.c., \tag{2.5}$$

where lower case Roman indices from the start of the alphabet denote generations (not to be confused with the charge conjugation operator), g, h and λ are dimensionless couplings, and μ_{23} carries dimensions of mass. Note that we have here assumed there is only a single generation of the new fields, but this could be trivially extended to multiple generations. Next $\mathcal{L}^{new}_{scalar}$ contains the additional terms gauge invariance allows in the scalar potential given by:

$$\begin{gathered}\mathcal{L}^{new}_{scalar} = \sum_{n=1}^{3}\Big[\alpha_n\left(\overline{\phi_n}\phi_n\right)^2 + \beta_n\left(\overline{\phi_n}\phi_n\right)\left(\overline{H}H\right) + m^2_{Sn}\left(\overline{\phi_n}\phi_n\right)\\ + \left\{\gamma_n\left(\overline{\phi_n}\phi_n\right)\left(\phi_2 H\right) + h.c.\right\}\Big] + \delta_{12}\left(\overline{\phi_1}\phi_1\right)\left(\overline{\phi_2}\phi_2\right) + \delta_{13}\left(\overline{\phi_1}\phi_1\right)\left(\overline{\phi_3}\phi_3\right)\\ + \delta_{23}\left(\overline{\phi_2}\phi_2\right)\left(\overline{\phi_3}\phi_3\right) + \left(\epsilon_{23}\phi_2\phi_2\phi_3 + \epsilon_H\phi_2\overline{H}\phi_3 + h.c.\right),\end{gathered} \tag{2.6}$$

where m_{Sn}, ϵ_{23} and ϵ_H have dimensions of mass, with other couplings being dimensionless. In addition to ensure there are not one loop diagrams induced it is convenient to not allow any of the new scalars to pick up a VEV. Taking $m^2_{Sn} > 0$, this means we require $\alpha_n > 0$ also. Similarly $\mathcal{L}^{new}_{extra}$ contains the extra terms allowed involving fermions and contains:

$$\mathcal{L}^{new}_{extra} = \kappa_1 \overline{f_{2L}} f_{1R} \phi_2 + \kappa_{2gh} \overline{Q_g} u_h \phi_2 + \kappa_{3i} \overline{Q_i} f_{1R} \phi_3 + h.c., \tag{2.7}$$

where the κs are dimensionless couplings. Notice that most couplings arise from ϕ_2 which, except under $SU(3)$, transforms like the Higgs. This is a general feature: introducing new fields with quantum numbers similar to SM fields will lead to a large number of couplings and thus potential one loop and two loop diagrams. Such features generically make these models more difficult to work with. Finally $\mathcal{L}^{new}_{fermion}$ contains the mass terms for the new fermions. Their non-observation would suggest that $m_{fermion} \gg m_{electroweak}$. Accordingly rather than giving them a mass through a Higgs coupling, it is more natural to make them vector-like fermions. This implies introducing an f_{1L} and f_{2R} that transform identically to f_{1R} and f_{2L} respectively. Then the mass term is simply:

$$\mathcal{L}^{new}_{fermion} = \sum_{n=1}^{2} m_{Fn} \overline{f_n} f_n, \tag{2.8}$$

where $f_n = f_{nL} + f_{nR}$. With the full Lagrangian in place there are now a few additional features of the model we can check. Firstly it can be shown the Lagrangian has no new global symmetries that are independent of baryon number and hypercharge. Next choosing ϕ_1, f_1 and f_2 to carry $B = 1/3$, whilst ϕ_2 and ϕ_3 carry no baryon number we find that this model exactly conserves baryon number, so this model will not be subject to constraints like those from proton decay. On the other hand the model must violate lepton number to generate a Majorana neutrino mass and indeed with a choice of ϕ_1 to have $L = 1$ and all other new fields to carry no lepton number, we find that the only term that breaks lepton number is $h_f^2 \overline{f_{1R}} L_f \phi_1$ and this has $\Delta L = 2$. Note that it is incorrect to think of this term as the source of lepton number violation in this model, as other terms were used to set the lepton numbers of the new fields, in truth it arises from the full Lagrangian.

The final check is whether this model allows additional Majorana neutrino mass diagrams. From the above it is clear any such diagram must include the h_f^2 term as this is the only way it can satisfy the $\Delta L = 2$ requirement. Now the only other coupling for ϕ_1 in the model is the $g^1_{ab} \overline{L^c_a} Q_b \overline{\phi_1}$ term as featured in the original diagram. If there were a one loop diagram there would have to be a way of connecting Q and f_{1R} without using scalars other than the Higgs. This is because Higgs lines can be replaced by their VEV, whilst other scalar lines cannot by construction and could only be closed off through another loop. A Higgs coupling will allow one to convert Q to d and f_{1R} to f_{2L}, but there is no combination of these that can be connected in a Higgs. Thus we can conclude this model has no induced one loop contribution to neutrino mass. By a similar type of argument where all the possible couplings are considered, it is not hard to show that there is in fact an additional two loop diagram - but only one - and it is shown in Figure 2.2.

In summary we have outlined the details of an extension to the SM with five additional fields, where the neutrino picks up a Majorana mass at two loops according to the interference of two diagrams. The model is likely to have interesting LHC phenomenology. For example ϕ_1 is a leptoquark, coupling to leptons and quarks, and this type of particle is being looked for in the data [28]. Nonetheless before considering the details of experimentally testing this model, we must check that the neutrino mass is consistent with atmospheric limits and furthermore is what we expect from this operator.

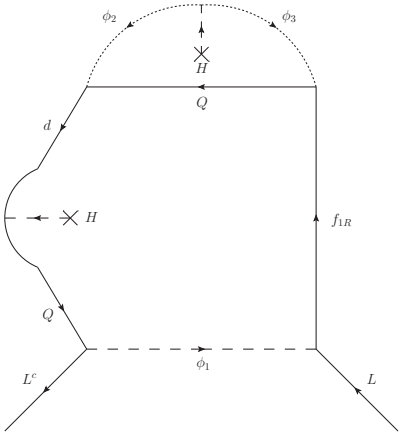

Figure 2.2: An independent two loop diagram.

2.1.2 Evaluating the Mass Matrix

To begin with observe that the generic radiative neutrino mass diagram can be visualised as in Figure 2.3, where the grey circle represents the loop structure. Now the induced coupling between $\overline{L_a^c}$ and L_b by such a diagram can be written as $\overline{L_a^c} P_L \mathcal{M}_{ab} L_b$, where a and b are generation indices, P_L emerges from the chirality structure of the fields, and $\mathcal{M}_{ab}$ is the neutrino mass matrix for this diagram. Accordingly to calculate this matrix from a diagram we need to to ignore the external L fields and calculate the Feynman amplitude of the internal loop structure.

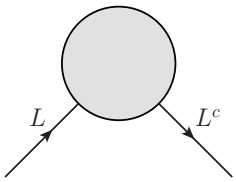

Figure 2.3: Generic radiative neutrino mass diagram.

Applying the Feynman rules to the first diagram (Figure 2.1) yields:

$$\begin{aligned} P_L \mathcal{M}^1_{ab} = \int \tfrac{d^4p}{(2\pi)^4} \int \tfrac{d^4q}{(2\pi)^4} \left(g^1_{ac} P_L\right) \tfrac{i\left(\not{p}+m_c\right)}{p^2-m_c^2} \left(g^2_{cd} P_L\right) \tfrac{i\left(\left[\not{p}-\not{q}\right]+m_d\right)}{(p-q)^2-m_d^2} \left(h^1_d P_L\right) \\ \times \tfrac{i\left(\not{p}+m_{f2}\right)}{p^2-m_{F2}^2} \left(v\lambda P_R\right) \tfrac{i\left(\not{p}+m_{f1}\right)}{p^2-m_{F1}^2} \left(h^2_b P_L\right) \tfrac{i}{p^2-m_{S1}^2} \tfrac{i}{q^2-m_{S2}^2} \left(v\mu_{23}\right) \tfrac{i}{q^2-m_{S3}^2}, \end{aligned} \tag{2.9}$$

where we have called the generation of the down-type quark on the left c and the one at the top d, the momentum in the lower loop is p and in the upper loop is q, and the integrals run over all possible momenta (i.e. $-\infty$ to ∞).

Now we can rearrange (2.9) by commuting the projection operators through, performing a Wick rotation, sending $q \to -q$, and using $\not{p}\not{p} = p^2$ to get:

$$P_L\mathcal{M}^1_{ab} = P_L\tfrac{iv^2}{(2\pi)^8}m_c m_d g^1_{ac}g^2_{cd}h^1_d h^2_b\lambda\mu_{23}\int d^4p\int d^4q p^2\tfrac{1}{p^2+m_c^2} \times\tfrac{1}{p^2+m_{F1}^2}\tfrac{1}{p^2+m_{F2}^2}\tfrac{1}{p^2+m_{S1}^2}\tfrac{1}{q^2+m_{S2}^2}\tfrac{1}{q^2+m_{S3}^2}\tfrac{1}{(p+q)^2+m_d^2} \tag{2.10}$$

From here it is clear that $\mathcal{M}^1_{ab}$ is just the parts on the right except for P_L and that the remaining work is in calculating the integral, which we label as I^1_{cd}. The exact details of how to calculate such integrals and the notation used below is outlined in appendix A and these techniques yield:

$$\begin{aligned} I^1_{cd} = {} & m^4_{S1}ACDG\left[(2m_{S1}|m_{S3}|m_d)-(2m_{S1}|m_{S2}|m_d)\right]+m^4_{F2}ABCF\left[(2m_{F2}|m_{S2}|m_d)-(2m_{F2}|m_{S3}|m_d)\right] \\ & +m^4_{F1}ABDE\left[(2m_{F1}|m_{S3}|m_d)-(2m_{F1}|m_{S2}|m_d)\right]+m^4_cAEFG\left[(2m_c|m_{S2}|m_d)-(2m_c|m_{S3}|m_d)\right] \\ & +m^2_{S1}ACDG\left[-m^2_{S2}\left(2m_{S2}|m_{S1}|m_d\right)-m^2_d\left(2m_d|m_{S1}|m_{S2}\right)+m^2_{S3}\left(2m_{S3}|m_{S1}|m_d\right)+m^2_d\left(2m_d|m_{S1}|m_{S3}\right)\right] \\ & +m^2_{F2}ABCF\left[-m^2_{S3}\left(2m_{S3}|m_{F2}|m_d\right)-m^2_d\left(2m_d|m_{F2}|m_{S3}\right)+m^2_{S2}\left(2m_{S2}|m_{F2}|m_d\right)+m^2_d\left(2m_d|m_{F2}|m_{S2}\right)\right] \\ & +m^2_{F1}ABDE\left[-m^2_{S2}\left(2m_{S2}|m_{F1}|m_d\right)-m^2_d\left(2m_d|m_{F1}|m_{S2}\right)+m^2_{S3}\left(2m_{S3}|m_{F1}|m_d\right)+m^2_d\left(2m_d|m_{F1}|m_{S3}\right)\right] \\ & +m^2_cAEFG\left[-m^2_{S3}\left(2m_{S3}|m_c|m_d\right)-m^2_d\left(2m_d|m_c|m_{S3}\right)+m^2_{S2}\left(2m_{S2}|m_c|m_d\right)+m^2_d\left(2m_d|m_c|m_{S2}\right)\right], \end{aligned} \tag{2.11}$$

where we use the shorthand $A=\left(m^2_{S2}-m^2_{S3}\right)^{-1}$, $B=\left(m^2_{F1}-m^2_{F2}\right)^{-1}$, $C=\left(m^2_{F2}-m^2_{S1}\right)^{-1}$, $D=\left(m^2_{F1}-m^2_{S1}\right)^{-1}$, $E=\left(m^2_c-m^2_{F1}\right)^{-1}$, $F=\left(m^2_c-m^2_{F2}\right)^{-1}$, and $G=\left(m^2_c-m^2_{S1}\right)^{-1}$. One can check this combination of integrals is convergent and accordingly integrals of the form $(2m|m_1|m_2)$ should be replaced with their *effective parts*, as explained in appendix A.

Repeating the same process as above for the second diagram (Figure 2.2), we find:

$$\begin{aligned} P_L\mathcal{M}^2_{ab} = {} & \int\tfrac{d^4p}{(2\pi)^4}\int\tfrac{d^4q}{(2\pi)^4}\left(g^1_{ac}P_L\right)\tfrac{i\left(\not{p}+m_c\right)}{p^2-m_c^2}\left(g^2_{cd}P_L\right)\tfrac{i\left(\left[\not{p}-\not{q}\right]+m_d\right)}{(p-q)^2-m_d^2}\left(\kappa_{3d}P_R\right) \\ & \times\tfrac{i\left(\not{p}+m_{F1}\right)}{p^2-m_{F1}^2}\left(h^2_bP_L\right)\tfrac{i}{p^2-m_{S1}^2}\tfrac{i}{q^2-m_{S2}^2}\left(v\mu_{23}\right)\tfrac{i}{q^2-m_{S3}^2} \end{aligned} \tag{2.12}$$

$$\begin{aligned} = {} & P_L\tfrac{-v}{(2\pi)^8}g^1_{ac}g^2_{cd}\kappa_{3d}\mu_{23}m_c\int d^4p\int d^4q\left(p^2-p\cdot q\right)\tfrac{1}{p^2+m_c^2} \\ & \times\tfrac{1}{p^2+m_{F1}^2}\tfrac{1}{p^2+m_{S1}^2}\tfrac{1}{q^2+m_{S1}^2}\tfrac{1}{q^2+m_{S3}^2}\tfrac{1}{(p+q)^2+m_d^2} \end{aligned} \tag{2.13}$$

The integral here has two parts; label the one with p^2 in the numerator as I^{2A}_{cd} and the one with $-p\cdot q$ as I^{2B}_{cd}. The first of these integrals can be evaluated using the techniques from appendix A. This was done, but the result is as long and ungainly as (2.11) so it is not presented here. The second integral cannot be evaluated in this manner. Whilst the numerator is odd, this does not imply the integral will vanish like it would for one loop integrals because the denominator is neither even nor odd due to the coupled $(p+q)^2$ propagator. We have evaluated I^{2B}_{cd} in appendix B.

Although this is mentioned in the appendix it is worth repeating that an important step in these calculations is determining whether the integrals converge. In this case I^1_{cd} and I^2_{cd} are convergent separately and this is because the two diagrams involve different couplings, which implies their divergent terms are linearly independent and so must cancel separately. Of course this will not always be the case. If two different diagrams have the same couplings it may require the combination of both to check all divergences cancel. Either way convergence works not only as a necessary step but is also a good check that the algebra has been calculated correctly.

2.1.3 Numerical Evaluation of the Mass

With an analytic expression for the integral we can put this into Mathematica and figure out the predicted neutrino mass, $m_\nu = |M^1_{ab} + M^2_{ab}|$. Given this is a model from an 11D operator the atmospheric limit of 0.05 eV may be problematic. To get the biggest mass out of our model we take the mass of the down type quarks to be the bottom mass ≈ 4.2 GeV.

Before getting a value, however, we still need to fix the coupling constants. In truth these couplings will be constrained by non-observation of rare processes like $\beta\beta0\nu$ or $\mu \to e\gamma$, yet at this stage we have not considered such limits in detail. Nevertheless it seems these constraints generically require most couplings to be between 0.1 and 0.01, see e.g. [29]. Accordingly at this first stage we take all couplings to be 0.1. The only exception is the massive coupling μ_{12}, which we take to be 0.1 times the average of m_{S2}, m_{S3} and m_{Higgs}. We can now reasonably use experimental values for the last number of around 126 GeV [30, 31].

Now taking all new particles to be of order 100 TeV (the masses cannot be degenerate or the analytic expressions diverge) we find $m_\nu \sim 0.1$ eV, which is in no danger of the atmospheric limit as we can always increase the couplings. This is higher than expected as de Gouvêa and Jenkins' analysis suggested that for $\mathcal{O}_{68_b}$ to fit the atmospheric limit, the new particle must have masses around 100 TeV with all couplings assumed to be around unity. Indeed taking couplings of order 1 the model can support $m_\nu \sim 1$ eV even with all new particles around 10^6 TeV.

To try and determine what is going on here we isolated the different contributions to the mass and quickly realised that on essentially the entire parameter space $\mathcal{M}^2 \gg \mathcal{M}^1$. For example when all new particles were around 1 TeV, $\mathcal{M}^2 \sim 10$ eV, whilst $\mathcal{M}^1 \sim 10^{-6}$ eV. Despite this if we take couplings of order 1 along with TeV masses, then we get $\mathcal{M}^1 \sim 0.1$ eV, which is much more in line with their suggestion. It seems that the second diagram, which was required for the consistency of our model, has made the original diagram ignorable as far as neutrino mass is concerned. We will try and understand this problem in the next section.

2.1.4 Analysing the Large Mass Problem

The above realisation calls for a careful consideration of this second diagram. Looking carefully back at Figure 2.2, note that if we treat the $\overline{Q}dH$ line on the left as a single d line - not unreasonable given this is how it is treated in the Feynman amplitude - we see that when we integrate out the new physics, the diagram reduces to an operator other than $\mathcal{O}_{68_b}$. Specifically it reduces to:

$$\mathcal{O}_3 = LLQd^cH \tag{2.14}$$

where we have left out the $SU(2)$ indices as it is impossible to distinguish between the different possibilities just from this diagram. de Gouvêa and Jenkins list the scale of new physics for $\mathcal{O}_3$ as between 10^5 and 10^8 TeV, but this was assuming a one loop model. If we add a further $16\pi^2$ suppression for an extra loop, then we are still between 10^3 and 10^6 TeV, so it is not surprising that this operator would dominate over $\mathcal{O}_{68_b}$.

Despite this it is not correct to say that the model we outlined above is actually a model of $\mathcal{O}_3$, because Figure 2.2 contains no f_2 and if it were the starting point, it would never have led

to Figure 2.1. It appears to be a composite model of both of the operators, but unfortunately it is emerging in such a way that $\mathcal{O}_{68_b}$ appears largely irrelevant. Given our initial aim of creating an 11D operator model, this model looks like it will not be useful. Any limits on this model will be dominated by the 7D $\mathcal{O}_3$ and so is unlikely to provide insights we can generalise to help rule out 11D models.

To try and understand how this problem emerged, consider the original operator again and observe that it can be rearranged as:

$$\mathcal{O}_{68_b} = \left(L^i L^j Q^k d^c H^l \epsilon_{ik} \epsilon_{jl}\right) \left(Q^r d^c \overline{H}_r\right) = \left(\mathcal{O}_{3_b}\right) \left(Q^r d^c \overline{H}_r\right) \ , \tag{2.15}$$

so $\mathcal{O}_{68_b}$ contains $\mathcal{O}_{3_b}$ and this is somehow emerging in the model we created. This type of structure applies for all operators from 61-75; they are the product of lower dimensional operators with SM terms. At first glance this problem appears unavoidable. If we introduce a new symmetry to forbid $LLQd^cH$ then this term would have to be odd under this symmetry. Then to ensure $\mathcal{O}_{68_b}$ is even and thus allowed, $Qd^c\overline{H}$ would have to be odd as well and thus forbidden. But a new model will not be particularly successful if it forbids SM couplings and thus this approach is futile.

Babu and Leung in their paper gave a suggestion as to how to get around such limitations: non-trivial Lorentz contractions between the terms. This means we must have a diagram where the vertices cannot contain both Ls, which we already ensure, or Qd^c. This last one we had in our diagram and it may be the source of the problem. So it might seem we can avoid this constraint if we write down a diagram from $\mathcal{O}_{68_b}$ without Qd^c at any vertex.

We tried to write down a diagram from $\mathcal{O}_{68_b}$ without Qd^c at any vertex, however it was found that this is not possible for any of the six fermion UV completions listed by Volkas and Angel. To prevent both the Q and d^c from being at the same vertex one commonly has to use a Higgs, but then in diagram A there simply are not enough Higgs, in diagram B the resulting expression is forbidden by chirality or in diagram C such a diagram would induce a lower dimension one loop model. All other possibilities fail for various reasons.

Accordingly we conclude that it does not appear possible to write down a consistent model from $\mathcal{O}_{68_b}$ that will not be dominated by a lower dimensional operator. This means the operator will not be useful from our perspective of analysing models purely from 11D operators and so we move on to a new operator.

2.2 A Model from $\mathcal{O}_{31_a}$

The next model we consider is derived from $\mathcal{O}_{31_a}$. Again the choice of this operator was essentially accidental. Initially we worked with $\mathcal{O}_{32_a}$, as it has the highest scale of new physics amongst the 11D operators. Nevertheless this operator contains $\overline{(L^i)^c}\ \overline{H}_i$, which when expanded couples the neutrino to the charged component of the Higgs. The closure of the charged Higgs introduces an additional loop, meaning this operator cannot be completed in just two loops. Accordingly we chose $\mathcal{O}_{31_a}$ as it has a similar structure, yet can be closed in two loops. The operator itself has the form:

$$\mathcal{O}_{31_a} = L^i L^j \overline{Q}_i \overline{d}^c \overline{Q}_k \overline{u}^c H^k H^l \epsilon_{jl} = \left[\overline{(L^i)^c} \overline{Q}_i d\right] \left[L^j H^l \epsilon_{jl}\right] \left[\ \overline{Q}_k u H^k\right] \tag{2.16}$$

This operator does not have the structure of a lower dimensional operator multiplied with a SM coupling, so we should not run into the exact same problem as we saw for our first model. Completing this using diagram C as in Figure 1.6, we have:

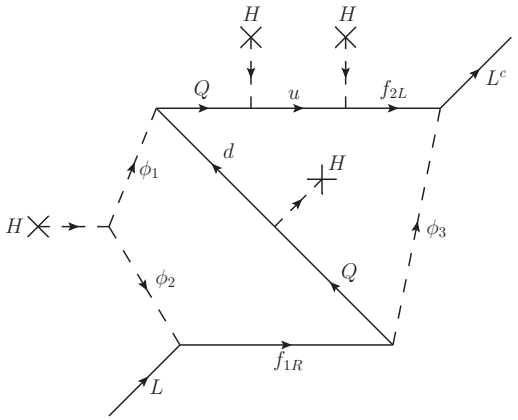

Figure 2.4: A model generated from $\mathcal{O}_{31_a}$.

Proceeding as above, this model has the following new particles:

$$\begin{aligned} \phi_1 &\sim (8,2,1) \\ \phi_2 &\sim (8,3,0) \\ \phi_3 &\sim \left(\overline{3},3,-4/3\right) \\ f_{1L/R} &\sim (8,4,-1) \\ f_{2L/R} &\sim (3,2,7/3) \end{aligned} \tag{2.17}$$

where $f_{1L/R}$ carries $L = 1$, ϕ_3 carries $L = 1$ and $B = -1/3$, whilst $f_{2L/R}$ carries $B = 1/3$. Otherwise the new particles carry no baryon or lepton numbers. The Lagrangian is written as:

$$\begin{aligned} \mathcal{L} &= \mathcal{L}^{SM} + \mathcal{L}^{new}_{kinetic} + \sum_{i=1}^{2} m_{Fi}\overline{f_i}f_i \\ &+ \Big[h^1_a\overline{f_{1R}}L_a\phi_2 + h^2_b\overline{Q_b}f_{1R}\overline{\phi_3} + g^1_{cd}\overline{Q_c}d_d\phi_1 + h^3_e\overline{f_{2L}}u_eH + h^4_f\overline{L^c_f}f_{2L}\phi_3 + \mu_{12}\overline{\phi_1\phi_2}H \\ &+\epsilon_{1H}\left(\phi_1\overline{H}\right)\left(\phi_1\overline{H}\right) + \epsilon_{112}\phi_1\overline{\phi_1}\phi_2 + \epsilon_{332}\phi_3\overline{\phi_3}\phi_2 + \epsilon_{222}\phi_2\phi_2\phi_2 \\ &+\kappa_{1g}\overline{u_g}f_{2L}\overline{\phi_1} + \kappa_{2hi}\overline{Q_h}u_i\phi_1 + \kappa_3\overline{f_{1R}}f_{1L}\phi_2 + \kappa_4\overline{f_{1L}}f_{1R}\phi_2 \\ &+\kappa_5\overline{f_{2R}}f_{2L}\phi_2 + \kappa_6\overline{f_{2L}}f_{2R}\phi_2 + \kappa_7\overline{f^c_{2L}}f_{1L}\phi_3 + \kappa_8\overline{f^c_{2R}}f_{1R}\phi_3 + h.c.\Big] \\ &+ \sum_{n=1}^{3}\Big[\alpha_n\left(\overline{\phi_n}\phi_n\right)^2 + \beta_n\left(\overline{\phi_n}\phi_n\right)\left(\overline{H}H\right) + m^2_{Si}\left(\overline{\phi_n}\phi_n\right) + \left\{\gamma_n\left(\overline{\phi_n}\phi_n\right)\left(\phi_1\overline{H}\right) + h.c.\right\}\Big] \\ &+\delta_{12}\left(\overline{\phi_1}\phi_1\right)\left(\overline{\phi_2}\phi_2\right) + \delta_{13}\left(\overline{\phi_1}\phi_1\right)\left(\overline{\phi_3}\phi_3\right) + \delta_{23}\left(\overline{\phi_2}\phi_2\right)\left(\overline{\phi_3}\phi_3\right) \end{aligned} \tag{2.18}$$

where $a - i$ denote generations, μ_{12}, m, ϵ_{112}, ϵ_{332} and ϵ_{222} carry dimensions of mass, and the other couplings are dimensionless. Again we assume the new fields only have one generation and take both α_i and m^2_{Si} to be positive to prevent the new scalars acquiring a VEV. There are three terms in the full Lagrangian that break lepton number, all with $\Delta L = 2$, and they are: $h^4_f\overline{L^c_f}f_{2L}\phi_3$, $\kappa_7\overline{f^c_{2L}}f_{1L}\phi_3$ and $\kappa_8\overline{f^c_{2R}}f_{1R}\phi_3$. Again we should think of this lepton number violation as arising from

the full Lagrangian, not just these terms. There are no terms that violate baryon number and again the Lagrangian has no new global symmetries. Finally the model allows four additional two loop diagrams:

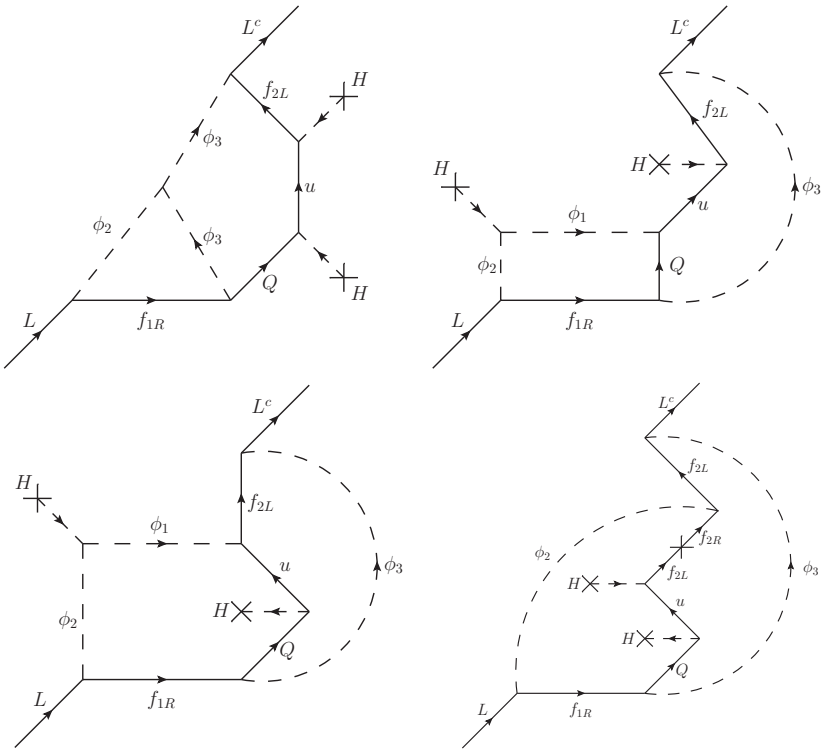

Figure 2.5: Additional Diagrams.

The above details demonstrate that we have written down a consistent model originating from $\mathcal{O}_{31_a}$ and so we could now calculate the mass associated with this model. Nevertheless it is possible to see that this model is going to run into problems before we even consider the mass. This is because the additional diagrams have a different structure to $\mathcal{O}_{31_a}$ - for example, none contain a d field. They can be thought of as originating from one of:

$$\begin{aligned} \mathcal{O}_4 &= LL\overline{Q}\overline{u^c}H \\ \mathcal{O}_6 &= LL\overline{Q}\overline{u^c}HH\overline{H} \end{aligned} \tag{2.19}$$

At two loops these operators both have a scale of new physics around 10^7 TeV and so would dominate over $\mathcal{O}_{31_a}$ - but perhaps not as strongly as we saw for the $\mathcal{O}_{68_b}$ model. We are again in a position where the model cannot really be considered a pure result of $\mathcal{O}_{31_a}$ and accordingly it will not be appropriate for our initial aim of examining generic 11D operators.

The failure of this model is not as easy to understand as for the previous case - $\mathcal{O}_{31_a}$ is not a product of lower dimensional operators. Nonetheless it appears that the non-trivial $SU(2)$ contractions that distinguish this operator from its potential substructures like $\mathcal{O}_4$, is not always enough to

prevent these operators arising. For example here whenever we couple H and u to a new fermion, we will always be liable to introduce the same particles in $\mathcal{O}_{31_a}$ as might appear in $\mathcal{O}_4$ or $\mathcal{O}_6$, which can in turn lead to these operators being induced.

2.3 Conclusions on 11D Operators

In the above two sections we have outlined two consistent and complete models originating from $\mathcal{O}_{68_b}$ and $\mathcal{O}_{31_a}$. Unfortunately neither one can be thought of as purely an 11D operator model and so they will not help us in the original aim of analysing the 11D spectrum. Nevertheless they have revealed some interesting features of the 11D landscape. Product operators (61-75) must use non-trivial Lorentz contractions or they will be dominated by one of their components parts. As we saw, however, this will not always be possible - there was no way to avoid this for $\mathcal{O}_{68_b}$. Concomitantly other 11D operators can also inadvertently invoke lower dimension diagrams. This failure is harder to rationalise, but it appears to be an example of a property that is common in radiative neutrino mass models. One usually has to choose the new particles carefully so as to not invoke a lower order model, for example avoid $f \sim (1,1,0)$ or the Type I Seesaw will arise. For the higher dimensional operators one has to choose particles such that none of the models from the 15 or so valid lower dimensional operators are invoked and generically this appears challenging. This raises the interesting possibility that it might simply be impossible to write down a consistent model that purely originates from an 11D operator, but this must be looked into more carefully.

As a final comment on 11D operators, in light of the above results we reconsidered which operators can be UV completed in two loops. As briefly noted, the $SU(2)$ structure plays an important role here - $\mathcal{O}_{32_a}$ can only be closed in three loops for this reason. The $SU(2)$ contractions do not appear to have been considered by Volkas and Angel, which would explain the difference between their list of operators that can be closed in two loops and that of de Gouvêa and Jenkins. Nonetheless after considering their list again, it appears de Gouvêa and Jenkins have also made a potential mistake in their analysis of the number of loops required for different operators. It appears they assumed two loop integrals with an odd numerator exactly vanish, like they would in the one loop case. This is patently false - see for example appendix B. Two loop integrals have a coupling propagator that is neither even nor odd and this negates such arguments. This assumption was used to justify why the operators 22, 27, 29b, 33, 39-42, 44-49 and 51 - except for 44c, 47f and 47h - can only be closed in three loops. Treating the integrals correctly would suggest these operators can be closed in two loops, which would increase the scale of new physics by $16\pi^2$ - roughly two orders of magnitude. The argument cannot be applied to reduce 44c, 47f and 47h to two loop closures due to the common structure $L^i L^j \epsilon_{ij} = \overline{L^c}^{\,i} L^j \epsilon_{ij} = \overline{\nu^c} e - \overline{e^c} \nu$. This structure means we cannot immediately obtain two external neutrinos as a mass diagram requires. We can fix this by converting e to ν through a charged Higgs coupling, but closing off this Higgs requires another loop. These operators should be able to be closed in three loops, however, rather than the four de Gouvêa and Jenkins suggest. Drawing on this conclusion we now have a new list of operators that require more than two loops in their UV completion: 15-20, 24, 28, 30a, 32, 34-38, 43, 44c, 47f, 47h, 50, 52-60, 63a, 64b, 65, 68a, 69b, 70, 73a, 74b and 75.

3 Constraints on Six Fermion Models

In the process of coming up with the two models outlined in the previous section, it was discovered that not all of the UV completions listed by Volkas and Angel are actually possible. Instead there are a number of constraints on what models are possible for different operators. The constraints were uncovered in a somewhat piecemeal fashion and they have been listed in a similar manner below. The only ordering principle is that these all apply to six fermion models and are either restrictions to avoid induced one loop models or alternatively restrictions on chirality.

3.1 Induced One Loop Models

If a two loop model allows neutrino mass to be generated at one loop level, then this single loop diagram will almost certainly dominate. Furthermore as the two loop diagram will usually act as a correction to the one loop diagram, its contribution will be divergent. For these reasons such models must be avoided. Several situations where this problem can arise are outlined below.

3.1.1 Restriction on Scalar Completion

For certain choices of the fermions at the top of the scalar UV completion, X and Y in Figure 3.1, the model will unavoidably lead to a one loop diagram of the form seen on the right of that figure.

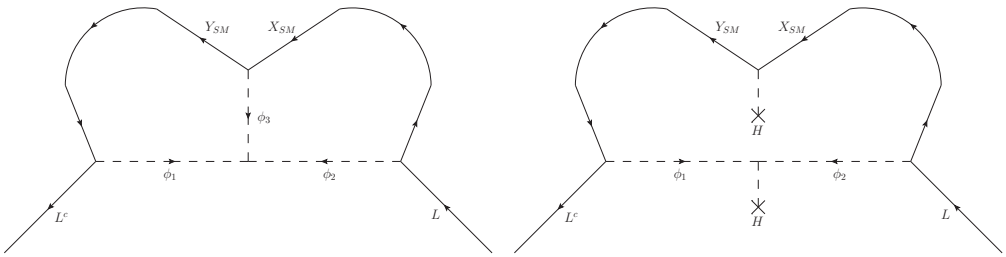

Figure 3.1: Original scalar completion (left) and potential one loop diagram (right).

The issue arises if X and Y are SM fields such that $\overline{Y}XH$ or $\overline{Y}X\overline{H}$ is invariant. In this case it is a simple check to see that ϕ_3 will be such that there must also be an invariant coupling of the form $\phi_1\phi_2 H$ or $\phi_1\phi_2\overline{H}$. These two couplings will mean there is also an allowed diagram where ϕ_3 is removed and replaced by two Higgs fields.

This issue can be most easily avoided by choosing X and Y so they do not couple to a Higgs. But if they do the one loop can only be avoided in the following way. If X and Y carry colour, then we can choose ϕ_3 to transform under the adjoint representation of $SU(3)$. In addition if we place a Higgs field on ϕ_3, then this will mean that there is no invariant coupling between ϕ_1, ϕ_2 and H. This Higgs insertion is clearly only possible for 11D operators and further will not hold if X and Y are colourless (e.g. L and e). This is because there will then be a coupling of the form $\phi_3 HH$, which gives a VEV to ϕ_3 and will similarly break the diagram down to one loop.

3.1.2 First Restriction on Completion via Diagram A, B and C

Consider the one loop diagrams in Figure 3.2, which can arise as subdiagrams in the fermion completions seen in diagram A, B and C. Despite what the diagram suggests, the solid lines need not be fermions. It turns out the argument below holds regardless of whether any of the lines are fermions or scalars, it has simply be drawn this way to give a concrete example.

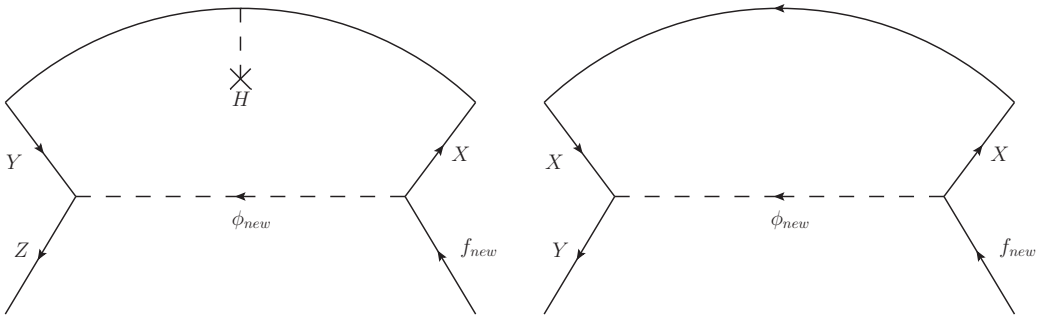

Figure 3.2: Problematic subdiagrams.

The issue is that these structures can give rise to an invariant coupling of the form $\overline{Z} f_{new} H$ (similarly for $\overline{H}$) for the diagram on the left and $\overline{Y} f_{new}$ for the one on the right. By considering the most general quantum numbers for the particles that allow the couplings as seen in the diagram, one can see that these lower order couplings can be avoided in two possible ways. In the case of the left hand diagram we can place a Higgs on the ϕ_{new} line and then the lower order coupling will not be allowed ($\overline{Z} f_{new} HH$ is not renormalizable). The other possibility is to choose the non-trivial $SU(2)$ quantum number for f_{new}. To understand this, one can show that in the case of the left diagram, $f_{new} \sim SU(2)_X \otimes SU(2)_Y \otimes SU(2)_Z$, but if X and Y couple to the Higgs, then $SU(2)_X \otimes SU(2)_Y \sim 2$ or 4. If we choose the 4 then $f_{new} \sim 4 \otimes SU(2)_Z$ and $\overline{Z} f_{new} H$ will not be invariant, forbidding the lower order coupling. An example of this second option is the diagram in Figure 2.2 from the $\mathcal{O}_{68_b}$ model. Here Z is d and we avoid the restriction because the $SU(2)$ number of f_{1R} is $4 \otimes 1 = 4$.

For the second diagram a similar argument reveals only the second option will avoid the problem. Naively one might think two Higgs could be placed on ϕ_{new} line, but if this is done it will not be possible to satisfy the chirality constraints on diagram A, B and C set out in the section below.

3.1.3 Second Restriction on Completion via Diagram A, B and C

The second possible issue that can arise for diagrams A, B and C is if the new fermion in these structures is such to allow a Majorana mass term $\overline{f} f^c$, and it is coupled to an L or L^c and a new scalar ϕ. In this case we can show there will be a further three couplings: $\overline{L} f^c \phi$, $\overline{f} L^c \phi$ and $\phi \phi HH$. These are sufficient to induce the one loop diagram in Figure 3.3, which originates from $\mathcal{O}_1$.

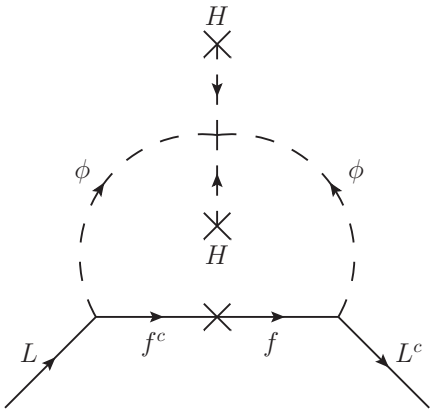

Figure 3.3: Induced one loop graph.

If a Higgs field is inserted to ensure the fermion is no longer connected to an L, then the one loop graph can be avoided. Similarly this one loop graph causes no problems in the case of diagram D1 or D2.

3.2 General Chirality Constraints

All the constraints in this section follow from the observation that $P_R P_L = P_L P_R = 0$. This puts a restriction on what fermions we can have meeting at a given vertex: for example $\overline{e_R} u_R = \overline{e} P_L P_R u = 0$ is forbidden, whilst $\overline{e_R} Q_L$ is allowed. Combining this observation with the fact that all Majorana neutrino mass diagrams must have the left handed L and right handed L^c externally provides a surprisingly strong restriction on what UV completions are allowed for certain six fermion operators.

A general observation that will be made use of below is that all six fermion operators that can be closed in two loops come in two classes. Class A operators have their external fermions closed off through a coupling with the Higgs; for example $\mathcal{O}_{12} = LL\overline{Q}u\overline{Q}u$, where we close off the loops using $\overline{Q}u\overline{H}$ couplings. Class B operators are closed off by just coupling a fermion field to its conjugate; for example $\mathcal{O}_{51} = LL\overline{u}u\overline{u}uHH$, where we close off the loops using $\overline{u}u$. The key point is that there are no operators where one pair of fermions is closed off as in class A and the other like in class B - both pairs are always closed off in the same way.

Below we will consider in turn each of the possible UV completions for six fermion operators, seen in Figure 1.4 and 1.6 - there is no need to consider the structure in Figure 1.5 separately as it is clear it is only allowed when there are two Higgs fields and they are used as in the diagram. But before doing so here are the two main conclusions that can be drawn from this analysis: 1. 9D six fermion operators can only be opened up using the scalar UV completion or a fermion completion where the new fermion can obtain a Majorana mass; and 2. Models can have up to three new fermions. Given the restriction on induced one loop models, the caveat listed on the first

conclusion can only apply to diagram D1 and D2. For an example of such a model see Volkas and Angel. As this can only occur for diagram D and the requirement that the new fermion can obtain a Majorana mass is quite strong, it is likely there are only a few models of this form. The second conclusion suggests chirality allows models with a large number of new fermions. As neutrino mass models traditionally do not have many associated new fermions, it would be interesting to see if a consistent model of this type can in fact be realised.

- *Scalar UV:* For either class A or B operators, looking at Figure 1.4 the diagram will not be forbidden by chirality if no Higgs are placed on the fermion line. This implies this structure can be supported by either 9D or 11D six fermion operators. In the 11D case it will also be possible to put two Higgs on the fermion line, but it will not be possible to just put one.

- *Diagram A:* In this case, the fermion line at the bottom creates a problem. This will only be non-vanishing if there is an extra chirality flip. This can either be brought about by inserting a Higgs somewhere on the line or alternatively making the new fermion a Majorana particle and using its mass term to induce a chirality flip. The latter option will induce a one loop diagram as seen above, so is not a valid option. The closed fermion loop at the top of the structure will be valid for either class A or B. Adding in a single extra Higgs that is available for 11D models will lead to forbidden vertices. Thus this completion is only allowed for 11D operators and always leads to three new scalars and two new fermions.

- *Diagram B:* For this diagram, working around the fermion line it can be seen that the chirality will not match up at either end unless a single Higgs is inserted somewhere for both class A and B operators. As above giving the new fermion a Majorana mass would lead to a one loop diagram, so we are restricted to 11D operators. Nevertheless in the 11D case, if there is a Majorana fermion the two Higgs can be placed on the fermion line to give a model with three new fermions. In the absence of a Majorana fermion, inserting two Higgs would again destroy the balance, so the second Higgs must be placed on a scalar and the model will have three new scalars and two new fermions.

- *Diagram C:* The analysis for this diagram is identical to that of diagram B.

- *Diagram D1:* In the case of class A operators the fermion line at the top of the diagram will be allowed by chirality, but the loop at the bottom will be forbidden. This problem can be avoided either by a Higgs insertion or alternatively using a Majorana mass term for the new fermion. This option can work for 9D or 11D operators. For class B operators the upper line will be forbidden, whilst the lower loop is allowed. This time the problem can only be fixed by a Higgs insertion at the top and so is only available to 11D operators.

- *Diagram D2:* In the case of class A or B operators the fermion line is invalid without an extra chirality flip. As mentioned this time it is possible either with a Higgs insertion or a Majorana mass for the new fermion, so is available to either 9D or 11D operators. Again with a Majorana fermion the 11D operators can give rise to models with three new fermions.

4 Testing the Zee-Babu Model at the LHC

As mentioned in section 1, the direct search for new particles from neutrino mass models at the LHC can provide important constraints on models and operators more generally. Indeed this class of constraints has not yet been explored and so the Melbourne group is seeking to play a pioneering role here. In this section we will use 7 TeV ATLAS data to perform a direct search for one of the particles from the ZBM. By setting strong limits on the particle mass, we seek to demonstrate the proof of concept that LHC data will play an important role in the general operator analysis. To begin with we provide a brief overview of the detector itself.

4.1 Overview of the ATLAS detector

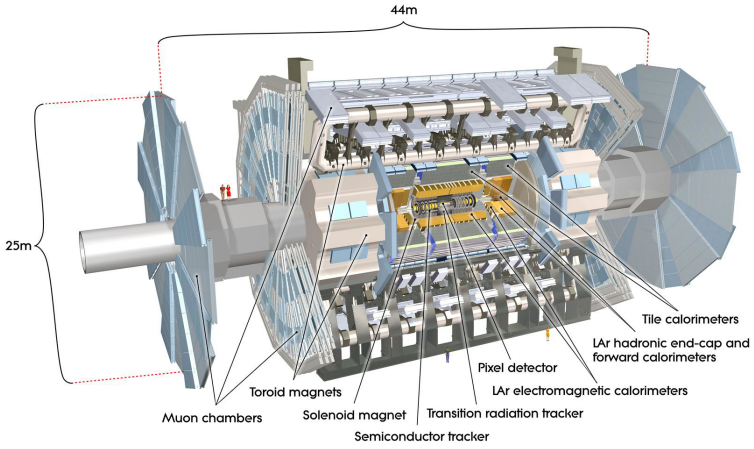

Figure 4.1: The ATLAS detector [32].

Figure 4.1 contains a graphical representation of the ATLAS detector with the key components labelled. The detector is made up of an inner tracking system, hadronic and electromagnetic calorimeters, and finally a muon spectrometer on the outside. The inner system surrounds the beam pipe at the interaction point and is made up of a set of mostly silicon detectors contained within a 2 T magnetic field. This system is used to track the path of particles just after the proton proton interaction; the magnetic field causes the trajectories of charged particles to curve, allowing their charge and transverse momentum to be calculated. The calorimeters are used to destructively measure the energy of the particles that pass through them. Finally the muon chambers are used to measure the path of the muons, which generally are not stopped in the inner parts of the detector.

Variables within ATLAS are defined with respect to a set of modified cylindrical coordinates where the z axis is taken along the beam pipe. Using these we can define the basic variables used throughout this section: p_T and E_T are the momentum and energy perpendicular to the beam pipe, and $\eta = -\log\tan(\theta/2)$, where θ is the polar angle measured from the positive z axis. It is

important to realise that while naively one would suspect p_T and E_T are trivially related through relativistic kinematics, they need to be considered separately as they are measured in different ways. As alluded to above p_T is calculated from the curvature of the particle's track, whereas E_T is determined using the energy deposited in the calorimeter.

The work done by the author in contribution to the results of this section mainly related to Monte Carlo (MC). MC provides a computer simulation of what a theory should look like in the detector - it bridges the gap between a Lagrangian and a muon energy distributions in the ATLAS detector. Testing a model at the LHC essentially boils down to comparing the MC of a given model to the data and so ensuring the MC behaves as we would expect it to appear in the detector is an essential step in any analysis. This process is referred to as *validation* of the MC.

There are a number of steps involved in the production of MC for a new physics model. Firstly the Lagrangian must be written into a Mathematica package called FeynRules, which calculates the Feynman rules associated with the model. The Feynman rules are then fed into MadGraph, which calculates the matrix elements that can be used to evaluate cross sections or decay widths. The program is then run through Pythia as this adds a more realistic treatment of several physical processes including weak boson decays or initial and final state radiation. Finally the corrected matrix elements are run through a model of the ATLAS detector to predict what the theory would look like in data.

4.2 Determining how to Test the Zee-Babu Model

4.2.1 Overview of the Zee-Babu Model

The ZBM is the archetypal two-loop radiative neutrino mass model. As explained in section 1 it can be derived from $\mathcal{O}_9$ and thus fits into the effective operator analysis. Furthermore we showed the neutrino mass diagram it generates in Figure 1.7. As can be seen there, the model introduces two new charged scalars that transform as $h^+ \sim (1,1,2)$ and $k^{++} \sim (1,1,4)$, which we will refer to as the k particle. This diagram induces the following Lagrangian [29, 33]:

$$\begin{aligned}\mathcal{L} \supset & \left(D_\mu h\right)^\dagger \left(D^\mu h\right) + \left(D_\mu k\right)^\dagger \left(D^\mu k\right) + \left[f_{ab}\overline{L_a^c} L_b h + g_{cd}\overline{e_c^c} e_d k - \mu \bar{h}\bar{h}k + h.c.\right] \\ & -m_h'^2 \left|h\right|^2 - m_k'^2 \left|k\right|^2 - \lambda_h \left|h\right|^4 - \lambda_k \left|k\right|^4 - \lambda_{hk} \left|h\right|^2 \overline{H}H - \lambda_{kH} \left|k\right|^2 \bar{H}H,\end{aligned} \tag{4.1}$$

where μ, m_h' and m_k' have dimension of mass, but other couplings are dimensionless. The masses of the new particles are combined from the mass term in the scalar potential, as well as the Higgs coupling terms, i.e. $m_i^2 = m_i'^2 + \lambda_{iH} v^2$. This Lagrangian requires h and k to carry two units of lepton number each. With this choice the μ term violates lepton number by two units, and ensures Figure 1.7 is a Majorana mass diagram.

A complete review of constraints on this model, including the prospects of direct detection at the LHC, is presented in [29]. For example, [34] has shown that the bound of $\mathrm{BR}\left(\mu \to e\gamma\right) \leq 1.2 \times 10^{-11}$ translates into a constraint on the h mass of $m_h \geq 160$ GeV. This branching ratio has since been improved by MEG [35] and so this limit could almost certainly be improved.

In this work we have focussed on setting limits on the k particle due to its clean detection signature. As explained in [29], if at first order we neglect the $\mu\bar{h}\bar{h}k$ coupling, then we would

expect pair production via $pp \to k\bar{k}$ as in Figure 4.2. As the k particle carries two units of lepton number, it will then decay into two same sign leptons denoted $\ell^{\pm}\ell'^{\pm}$. Thus its detection signature is same sign dilepton pairs, which can be considered clean for the following two reasons. Firstly there is limited SM background to our signal. There are no doubly charged particles in the SM and accordingly pair production of leptons occurs in opposite sign pairs, for example $Z \to e^+e^-$, rather than same sign pairs. Despite this there is a finite background from events where the charge of the lepton is misidentified, a jet is mistakenly reconstructed as a lepton, or from multilepton SM events such as $ZZ \to \ell^+\ell^-\ell'^+\ell'^-$. Secondly most of the backgrounds are leptonic, which occur several orders of magnitude less often than QCD processes at a proton proton machine like the LHC. While this means the signal is also not produced as often, the key quantity in any analysis is the signal to noise ratio and this substantially benefits from the background reduction.

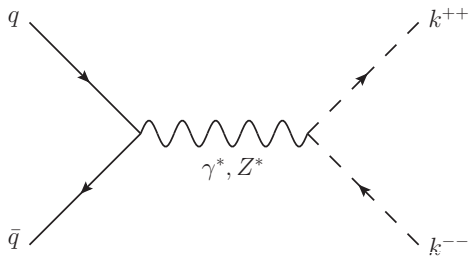

Figure 4.2: Pair Production of the k particle.

In line with the process outlined earlier we produced MC for both $pp \to kk \to \ell\ell\ell\ell$, which was used, but also $pp \to hh \to \ell\nu\ell\nu$, which was not. In order to validate our locally produced signal MC, we plotted distributions of many different variables for a large number of masses for the k particle. Any time a feature was seen in a distribution was not as expected, we would make sure we could trace its origin until it was either fixed or understood.

4.2.2 Fitting into an Existing Analysis

Although rare in the SM, same sign dileptons are predicted in a variegated collection of new physics models, including the left-right symmetric model, Higgs triplet model [36], little Higgs model [37], fourth-family quarks [38], supersymmetry [39] and universal extra dimensions [40]. These models are searched for in the same sign dilepton analysis, which aims to place limits on the anomalous (i.e. non-SM) production of same sign lepton pairs in a model independent way, and then subsequently perform a dedicated search for the left and right handed doubly charged Higgs (DCH) that appear in the left-right symmetric model.

This presented an opportunity for testing the ZBM as the k particle transforms exactly like the left handed DCH (denoted H_L), except that H_L is not a singlet under $SU(2)$. Nevertheless as the search simply looked for same sign leptons - it did not, for example, consider the possibility that either one might have come from a W - it seemed possible the limits on H_L might be directly transferable to the k particle.

In order to test this hypothesis we needed to compare the predictions of both models for key variables used in the same sign dilepton analysis. To do this we produced 10,000 MC signal events of $pp \to H_L H_L/kk$, which then decay into all possible combinations of electrons and muons. We did not consider topologies with taus as they have a large QCD background. For this reason we use the terminology common in experimental particle physics that a 'lepton' refers only to electrons and muons. In order to facilitate a concrete comparison, we set the mass of both particles to 200 GeV and their decay widths to 1 GeV. Note that whilst the two models would not predict these particles to have the same width, this is a parameter that can be scaled within the model - we can set limits for different widths - and so it is not unreasonable to match the two particles in this way.

The key variables chosen for the comparison were the p_T, η and the *invariant mass* of the two leptons, denoted $m(\ell\ell)$. These variables play a critical role in the same sign dilepton analysis and if the two models look the same in these variables then there would be no reason to suspect they should behave at all differently as far as the analysis was concerned. Before presenting the figures, it is important to note we do not simply plot the p_T of all leptons in the event. Rather as we are interested in same sign lepton pairs, we break the event into a set of all positively and negatively charged leptons. Within the smaller set of same sign leptons, we choose the lepton with the highest p_T and call it the *leading* lepton and that with the second highest the *subleading* lepton. The rationale for this is that these leptons are most likely to be the ones coming from the decaying k or H_L. Clearly this will not always be true, but to a good approximation it is as our MC contains mainly signal. The only backgrounds included in the sample are those simulated from initial and final state radiation as well as detector effects. Then we plot the p_T and η distributions for the leading and subleading leptons (combining the results from both charges). Finally the invariant mass distribution is the invariant mass of the leading and subleading lepton. These results are presented in Figure 4.3. Note in the invariant mass distribution we see a Breit-Wigner centred at the particle mass 200 GeV, which is exactly what we would expect for a reconstructed mass distribution of a particle with finite decay width and thus lifetime.

Figure 4.3 shows that as far as the key variables in this analysis are concerned, there is no difference between H_L and the k. This demonstrates that any limits set on the H_L could trivially be translated to the k. As our original aim was to set limits on the k, it was clear the best way to go about this was to join the same sign dilepton group and assist them in their analysis.

4.3 Overview of the Same Sign Dilepton Analysis

The aim of the same sign dilepton analysis was to update the 2010 1.6 fb^{-1} dimuon analysis [43] to include the full 2011 4.7 fb^{-1} dataset as well as all channels (ee, $e\mu$ and $\mu\mu$), and then to use this to set limits on the DCH. Both objectives were met and the results are published in [41, 42]. Note that although the author ultimately contributed to both papers, he is only listed as an author in the first due to the ATLAS rule forbidding anyone to be an author on more than one paper before completing their service work.

We have already noted that this search channel is well motivated by a number of new physics models including the ZBM. Also we pointed out that same sign dilepton events are rare in the SM and this means one can perform a low background search and constrain such models even if

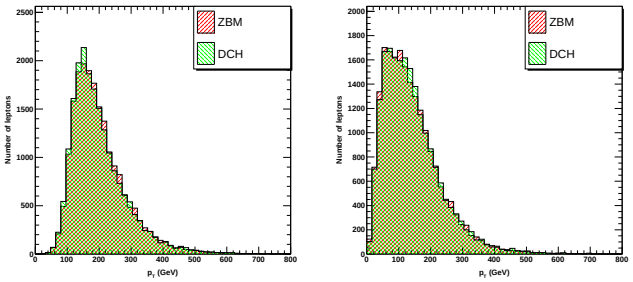

(a) Leading (left) and Subleading (right) p_T Distribution

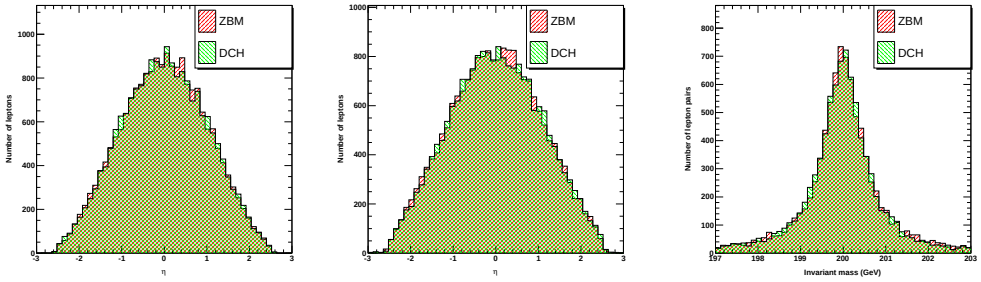

(b) Leading (left) and Subleading (right) η Distribution

(c) Invariant Mass Distribution

Figure 4.3: Comparison of the k and H_L in key variables.

they only predict a marginal enhancement over background. Nevertheless as there are many new models that could explain any excess, the analysis is careful to be as inclusive as possible. This means the analysis tries to use the minimal number of selection criteria, as particular cuts can be biased against particular models.

Below we provide a prospectus of the analysis as a whole. In all but the final subsection we will be explaining the work of the general search for anomalous production of same sign dilepton pairs, the details of which are contained in [41]. The final subsection outlines how the search was optimised for the doubly charged Higgs as in [42]. Throughout we place particular emphasis on work done by the author, which mainly related to the definition of the fiducial region and calculation of ϵ_{fid} explained in the limit setting subsection. Note the author was also involved in a number of smaller tasks including the request and validation of updated DCH MC, comparing the impact on MC of using different simulations of the ATLAS detector or parton distribution functions (PDFs), and calculating selection efficiencies for the DCH passing our selection criteria necessary for [42]. Nonetheless there is not room here to go into these smaller tasks.

4.3.1 Backgrounds

Although same sign lepton pairs occur rarely in the SM and we will set up our event selection to minimise contamination from potential backgrounds, there are no zero background searches and even if they are small, the backgrounds here must be carefully considered if we are to distinguish them from a signal. There are three dominant sources of background in this analysis: prompt, charge-flip and non-prompt or 'fakes'. We discuss each in turn below.

The prompt background arises from the SM directly creating our signal - two same sign leptons. Prompt refers to the fact these leptons originate from the decay of relatively short lived particles; non-prompt leptons come from more complicated and thereby longer decay chain (for example a lepton emerging from a jet). In the standard model these can arise from the production of WZ, ZZ and to a lesser extent $W^{\pm}W^{\pm}$, $t\bar{t}W$ and $t\bar{t}Z$. For example we could have $pp \to ZZ \to e^{+}e^{-}\mu^{+}\mu^{-}$ and this would be a clear background to our signal. The size of this background is determined from MC samples.

The charge-flip background occurs when there is a misidentification of a charge of one of the leptons. This can occur for a high momentum particle as the detector is unable to resolve the curvature of the track. Studies on $Z \to \mu\mu$ determined the effect is completely negligible for muons and thus this is only a background for electron final states. For the electrons the background is estimated from MC, but this process does not get the size exactly correct. The size is corrected by scaling MC to agree with data using $Z \to ee$ in the Z mass window.

Finally the non-prompt or fake background arises where a lepton emerges from a hadronic decay or misidentification. A number of processes can contribute to this such as $W+$ jet, $Z+$jet, multi-jet, and $t\bar{t}$ production. For example in $Z+$jet, the Z could decay to $\ell^{+}\ell^{-}$ and if the jet then fakes a lepton, we have a background that might pass our selection criteria. The underlying processes for these backgrounds are related to QCD, and because hadron machines like the LHC produce QCD events so regularly, even if a jet faking a lepton is rare this can be a considerable background. It also makes approximating this background via MC unrealistic because of how much would be required. Accordingly we use procedures known as 'data driven' techniques to estimate this background. In essence the size of the background is estimated in a region that is orthogonal to the region defined by our event selection, outlined below, so that we can be confident it will not be contaminated by our signal. The orthogonal region is determined by simply inverting one of the event selection cuts. Once the background is estimated in this region it is then scaled back to our event region to get an approximate size of the background. The actual details, however, are quite technical and interested readers are referred to the paper for further information.

4.3.2 Event Selection

The aim of event selection is to define a selection criteria in a way that maximises our signal to noise ratio. To begin with we have to decide how to choose our electrons, muons and jets. This is because the detector does not 'see' particles, rather it measures quantities like hits in its tracking system or energy depositions in the calorimeters. We then need to impose algorithms that convert from this raw information to physical objects like an electron. There are a number of standard algorithms used for these throughout ATLAS. For the leptons we selected only the cleanest particles. This

means we potentially throw away a number of candidate events, but it reduces the possibility of contamination by misidentified particles - one of our key backgrounds. As seen, jets can form background to our signal in two ways: a jet fakes a lepton or alternatively a lepton forms part of a jet. In order to catch this as often as possible, we choose the algorithm that catches the most number of jets, even though it is not the cleanest.

Next we need to ensure we are not selecting leptons that have come from background noise, which occurs because colliding bunches of protons creates a busy environment in the detector. This is done by requiring leptons to have high p_T and a central η, which suggests they came from a hard scattering event. Specifically we require at least two electrons or muons with the same charge that have $p_T > 20$ GeV. If the leading lepton is an electron, we also require it had $p_T > 25$ GeV. Muons must have $|\eta| < 2.5$, whereas electrons must have both $|\eta| < 2.47$ but not $1.37 < |\eta| < 1.52$. This excluded region is referred to as the *crack* and is removed as the electronics in this section have poor electron reconstruction. In addition we require that the candidate leptons both originate from near the same vertex. This is done as again it biases against leptons that were not created from the same particle.

A further criteria that biases against background is to require the particles to be isolated from other activity, as this prevents picking up leptons that might have originated from a jet, for example. Although the probability for this occurring might be quite small, as QCD processes occur with enormous regularity in the LHC, this cut is one of the most important in maximising signal to background in our analysis. Furthermore this criteria was quite important in the work of the author on limit setting and so we will explain it in a bit of detail. To begin with the standard way of determining if two objects are near each other in the detector is to measure the difference in the angular position between their tracks - $\Delta\eta$ and $\Delta\phi$ - and form the following cone size variable:

$$\Delta R = \sqrt{(\Delta\eta)^2 + (\Delta\phi)^2} \tag{4.2}$$

The larger we require the ΔR separation to be between the particles, the more isolated they must be. Then to avoid the known issue of counting jets as an electron, we veto any electron within $\Delta R = 0.2$ of a jet with $p_T > 25$ GeV and $|\eta| < 2.8$. Furthermore all lepton candidates must be separated by at least $\Delta R > 0.4$ from any jet with $p_T > 25$ GeV $+0.05 \times p_T(\ell)$ and $|\eta| < 2.8$.

A further isolation type criteria that is used to remove leptons that are more likely to be due to background requires the introduction of two new variables: $E_T^{cone\Delta R_{iso}}$ and $p_T^{cone\Delta R_{iso}}$. These variables are defined for a given particle as the sum of the E_T or p_T of all objects in a cone of size ΔR_{iso} around the particle, without including the original particle itself. As p_T is measured from the bend in the particle track, it turns out only charged particles with $p_T > 1$ GeV contribute to $p_T^{cone\Delta R_{iso}}$. If either variable is too large, it would suggest there is a lot of activity around the lepton and thus it is more likely to have come from some complicated background event rather than a simple new physics process. Cuts on these variables have been optimised for signal over background and for this analysis we require for electrons:

- $E_T^{cone0.2} < (3 + (p_T(e) - 20) \times 0.037)$ GeV; and
- $p_T^{cone0.3}/p_T(e) < 0.1$.

The E_T^{cone} variable is particularly susceptible to the amount of background noise in the detector, as it adds in everything within the cone. This noise is referred to as *pileup* and we have to correct E_T^{cone} for the amount of pileup in the detector and this becomes more difficult as the rate of collisions increases. For muons we instead require:

- $p_T^{cone0.4}/p_T\,(\mu) < 0.06$, if $p_T\,(\mu) < 100$ GeV; or
- $p_T^{cone0.4} < (4 + p_T\,(\mu) \times 0.02)$ GeV, if $p_T\,(\mu) > 100$ GeV.

Finally we place two requirements on the invariant mass of the candidate same sign dilepton pair. Firstly we require the invariant mass to be greater than 15 GeV. This is because none of the new particles are expected to be this light, but some of the backgrounds are. Secondly if both leptons are electrons we veto those with an invariant mass in the range 70-110 GeV. This is done as this window was used to calibrate the charge flip background, but also as it is roughly the Z boson mass and it reduces the background from $Z \to e^+e^-$ where one of the charges of the electrons is misidentified.

There are also several technical requirements such as trigger matching of the leptons. We have not outlined these as it is not as transparent why they are necessary and also they do not have a substantial impact on the selection. Nevertheless note that we have not set, for example, any cuts on the number of jets in the event. This is because, unlike the ZBM, some new physics models predict jets in addition to like sign dileptons and such cuts would be against the spirit of inclusiveness.

4.3.3 Systematics

Although it has not been mentioned so far, of course all experimental values will be accompanied by a statistical and systematic error. Calculating the systematic uncertainties is a challenging process and often one of the most carefully considered aspects of an analysis.

Uncertainties can enter into the values in a number of different ways. For example the error in the luminosity of $\pm 3.9\%$ translates into an error on the number of events we have for values approximated from MC. The MC for SM backgrounds also acquires an uncertainty from two more sources: 1. An error in the cross section due to higher-order corrections, which is, for example, estimated at $\pm 10\%$ for WZ and ZZ; and 2. An error in the PDFs of $\pm 7\%$. Note PDFs are crucial in determining the outcome of a proton proton collision. There are also errors associated with fundamental objects like our lepton identification. Such errors can be approximated from well understood processes like Z decays and results in an uncertainty on the number of like-sign pairs of $\pm$(3-4)%. Several other important sources of error include the uncertainty in the electron energy of $\pm 1\%$ and in how often charge misidentification occurs for electrons, which varies between $\pm 15\%$ and $\pm 23\%$ for different invariant mass ranges. The analysis treats all of these uncertainties carefully and they are translated into errors on final results.

4.3.4 Results

Next we look at the actual data to count the number of events that pass our event selection and compare this to our background estimates with error. This is done for each final state separately. The values in Table 1 are given for different regions of invariant mass of the lepton pairs, as higher mass new particles would be easier to observe in the higher mass windows. Also in Figure 4.4 we present the invariant mass distribution for the different final states. Both of these are taken directly from [41]. None of these results suggest any substantial deviation from the expected background. Note that we also looked at positive and negative pairs separately and again observed no significant deviation.

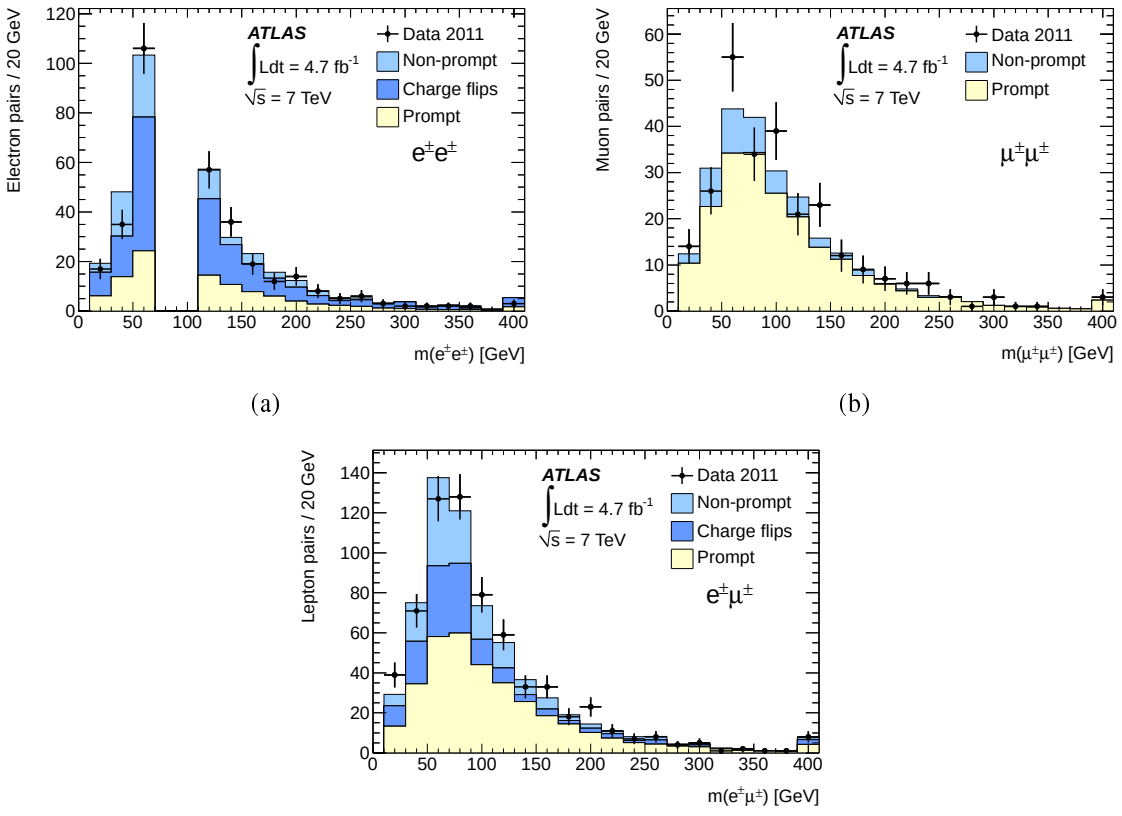

Figure 4.4: Invariant mass distributions for (a) ee, (b) $\mu\mu$, and (c) $e\mu$ pairs passing the full event selection. The data is represented by the closed circles, whereas the background is represented by the stacked histograms.

Table 1: Comparison of data to background expectation for same sign lepton pairs in the region defined by our event selection.

Sample	Number of electron pairs with $m(e^{\pm}e^{\pm})$				
	> 15 GeV	> 100 GeV	> 200 GeV	> 300 GeV	> 400 GeV
Prompt	101 ± 13	56.3 ± 7.2	14.8 ± 2.0	4.3 ± 0.7	1.4 ± 0.3
Non-prompt	75 ± 21	28.8 ± 8.6	5.8 ± 2.5	$0.5^{+0.8}_{-0.5}$	$0.0^{+0.2}_{-0.0}$
Charge flips and conversions	170 ± 33	91 ± 16	22.1 ± 4.4	8.0 ± 1.7	3.4 ± 0.8
Sum of backgrounds	346 ± 44	176 ± 21	42.8 ± 5.7	12.8 ± 2.1	4.8 ± 0.9
Data	329	171	38	10	3
	Number of muon pairs with $m(\mu^{\pm}\mu^{\pm})$				
	> 15 GeV	> 100 GeV	> 200 GeV	> 300 GeV	> 400 GeV
Prompt	205 ± 26	90 ± 11	21.8 ± 2.8	5.8 ± 0.9	2.2 ± 0.4
Non-prompt	42 ± 14	12.1 ± 4.6	1.0 ± 0.6	$0.0^{+0.3}_{-0.0}$	$0.0^{+0.3}_{-0.0}$
Charge flips	$0.0^{+4.9}_{-0.0}$	$0.0^{+2.5}_{-0.0}$	$0.0^{+1.8}_{-0.0}$	$0.0^{+1.7}_{-0.0}$	$0.0^{+1.7}_{-0.0}$
Sum of backgrounds	247^{+30}_{-29}	102 ± 12	$22.8^{+3.4}_{-2.9}$	$5.8^{+1.9}_{-0.9}$	$2.2^{+1.7}_{-0.4}$
Data	264	110	29	6	2
	Number of lepton pairs with $m(e^{\pm}\mu^{\pm})$				
	> 15 GeV	> 100 GeV	> 200 GeV	> 300 GeV	> 400 GeV
Prompt	346 ± 43	157 ± 20	36.6 ± 4.7	10.8 ± 1.5	3.9 ± 0.6
Non-prompt	151 ± 47	45 ± 13	9.2 ± 4.1	2.6 ± 1.1	1.0 ± 0.6
Charge flips and conversions	142 ± 28	33 ± 7	10.5 ± 2.8	2.9 ± 1.2	2.2 ± 1.1
Sum of backgrounds	639 ± 71	235 ± 25	56.4 ± 7.0	16.3 ± 2.3	7.0 ± 1.4
Data	658	259	61	17	7

4.3.5 Limit Setting

As the data is entirely consistent with the expected background, we use the results to set a limit on the production of new physics. The first step is to determine a 95% confidence level (CL) for the upper limit on the number of events in the different invariant mass windows, denoted N_{95}. The standard practice in ATLAS is to use the CL_s method [44].

Now naively one might think we could translate this directly to a limit on the cross section using $\sigma_{95} = N_{95}/\left(A \times \epsilon \times \mathscr{L}\right)$, where $A \times \epsilon$ is the acceptance times efficiency and $\mathscr{L} = \int \mathcal{L} dt$ is the integrated luminosity (specifically 4.7 fb^{-1} here). $A \times \epsilon$ is required as σ_{95} is the cross section for production anywhere in the detector, but N_{95} is a result of the number of events counted in the event region. The event region does not cover the entire detector, for example there are cuts on η, and the fraction of the detector covered by the analysis is the acceptance A. Furthermore not all same sign dilepton pairs in this region are detected because of the selection criteria; the efficiency for detecting such pairs is reflected in ϵ and is a function of our selection criteria. Nevertheless as should be clear the limit here is critically dependent on the event selection cuts. This region has been defined using variables that theorists external to ATLAS do not have access to, for example the pileup corrected E_T^{cone}. For this reason a theorist would not be able to calculate what ϵ should be for their model and thus such a naive cross section limit would be useless.

The way around this is to define a new region of phase space, called the *fiducial region*, solely in terms of criteria theorists can apply themselves. By setting a limit in a region where the theorists can calculate what the cross section of their model is, the limit becomes usable. Like the event selection region, the fiducial region is defined by a series of cuts. In order to determine what the criteria should be it is useful to introduce the model dependent parameter ϵ_{fid}, called the *fiducial efficiency*, which quantifies how similar the fiducial and selection regions are. To evaluate this quantity we take signal MC from a specific model and calculate the following ratio:

$$\epsilon_{fid} \equiv \frac{\text{Number of pairs that pass both the fiducial region and event selection criteria}}{\text{Number of pairs that pass the event selection criteria}} \times 100 \quad (4.3)$$

Once this is evaluated, we can define a more meaningful limit:

$$\sigma_{95}^{fid} = \frac{N_{95}}{\epsilon_{fid} \times \int \mathcal{L} dt} \quad (4.4)$$

where σ_{95}^{fid} is the 95% CL upper limit on the cross section in the fiducial region, not the entire detector so there is no acceptance factor. Nonetheless the limit obtained is critically dependent on ϵ_{fid} and thus the definition of the fiducial region. The idea is to optimise the fiducial region criteria according to the following principles:

- Maximise the fiducial efficiency in order to set the strongest limit via (4.4);
- Minimise the *leakage*, which is defined as the number of events that pass the selection criteria, but not the fiducial criteria, divided by the number that passed selection times 100. In this sense it is orthogonal to the fiducial efficiency and if it is large this would suggest strong disagreement between the selection and fiducial regions;

- Ensure the fiducial efficiency is relatively flat across different models and masses within models. As we consider models with a number of different final state topologies, this ensures that our conservative limit should be applicable even to models not considered; and
- The cuts themselves should not be overly complicated as this introduces the possibility that theorists trying to set limits on their models could misuse them.

The third point listed was the primary focus of the analysis as it gives confidence the limit is transferable to models not considered, but each played a part in guiding the process. Naively it would seem the best way to maximise ϵ_{fid} would be to make the selection and fiducial region as similar as possible. Yet as theorists only have access to the 4-vectors of the different particles, this is all we can use to define criteria similar to the those in event selection. Note as mentioned ϵ_{fid} was calculated for a number of different models. We used theories with various topologies, specifically with a wide range of jet multiplicities and lepton momenta. The models considered were a DCH for masses between 50 and 1000 GeV, fourth generation quarks decaying to Wt with masses from 300 to 500 GeV, like-sign top-quark production via a contact interaction, and a right handed W of mass 800 to 2500 GeV, which then decays to same sign leptons and a right handed neutrino.

As a starting point in the definition of the fiducial region, the selection cuts on the simplest variables - p_T, η and $m(\ell\ell)$ - were exactly mimicked from the event region cuts. There was no reason to suspect modifying such simple cuts would help with any of our aims. Now the previous $\mu\mu$ analysis had augmented these simple cuts with a jet isolation requirement; it did not include any of the p_T^{cone} or E_T^{cone} criteria involved in event selection. Nevertheless as mentioned under event selection, these cuts play a key role in suppressing QCD backgrounds. It was thought that finding a way to include these variables into the fiducial region would substantially improve performance, given their importance in the selection region. We'll discuss each of these below.

To define $p_T^{cone\Delta R_{iso}}$ for a given lepton using 4-vectors only, we calculated the ΔR between all charged particles and the lepton using (4.2), and then added up the p_T for those with $\Delta R \leq \Delta R_{iso}$ and $p_T > 1$ GeV. Note that one must be careful to ensure the p_T of the original lepton is not included and also that the same particle is not added several times. This second point is more subtle than it may appear. If, for example, a particle undergoes Bremsstrahlung in the detector (e.g. $e \to e\gamma$) then as the program treats the particle before and after this event separately, one can end up adding it twice. To remove this possibility we only added in stable particles and disregarded particles that emerged from detector interactions.

With the above definition settled we implemented the $p_T^{cone\Delta R_{iso}}$ cuts exactly as in the selection criteria. It turned out these had a substantial impact: they led to a higher ϵ_{fid}, reduced leakage and increased uniformity across models and masses. The definition was perhaps a bit complicated, but given the benefit to other considerations it was decided it was worthwhile to include. Furthermore it was realised that now the jet isolation cut was redundant - the $p_T^{cone\Delta R_{iso}}$ cut caught almost all non-isolated leptons.

E_T^{cone} did not share the same elegant properties. It was defined similarly to p_T^{cone}, but we added in all particles rather than just charged ones. This time we needed to be careful to remove neutrinos, as these would not be detected anywhere in the ATLAS detector, let alone the calorimeters, and so would not contribute to the selection values. Unfortunately when this variable was added

the leakage values increased substantially, some models produced values greater than 30%. For comparison the leakage would ideally only be several percent.

In order to determine what was going on, we sought to compare our fiducial definition of E_T^{cone} to the selection version, created by the ATLAS analysis code. In order to do this we calculated the E_T^{cone} in the two different ways for the most energetic lepton in each event from the 50 GeV DCH MC sample. We then plotted them against each other in a 2D scatter plot. If our fiducial definition was working accurately, there should be a strong correlation between the two values. As can be seen in Figure 4.5, this is not the case. We have only shown the values here over a small energy range, but the result is typical of what was seen: there was no correlation between the variables.

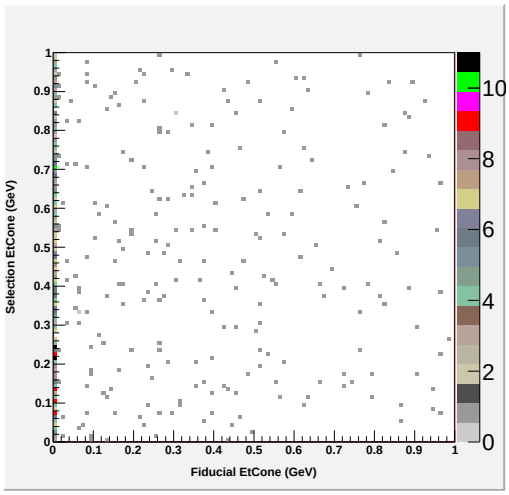

Figure 4.5: Correlation between Selection and Fiducial E_T^{cone}.

As noted earlier, E_T^{cone} is particularly sensitive to pileup. As our fiducial definition makes no attempt to account for this, it was suspected that this was causing the difference between our fiducial and selection region and thus a large leakage. We investigated the possibility of modelling pileup in the fiducial criteria, but ultimately it was concluded any available option would be much too complicated to pass our simplicity requirement. For these reasons it was decided we would leave out E_T^{cone} from the fiducial region. As an aside this highlights that one must be careful when trying to recreate complicated ATLAS cuts just from 4-vectors.

Accordingly we define our fiducial region using cuts on same sign pairs to include an invariant mass cut of $m(\ell\ell) > 15$ GeV, a veto on 70 GeV $< m(ee) <$ 110 GeV and the cuts on individual leptons listed in Table 2. Using these cuts it was simply a matter of calculating ϵ_{fid} and the leakage for all the different models and masses. This was done and from these values we conservatively selected the lowest fiducial efficiency values of 43% for ee, 55% for $e\mu$ and 59% for $\mu\mu$. The new fiducial region represented a significant improvement over the previous $\mu\mu$ analysis in essentially all criteria. The lowest fiducial efficiency we had for $\mu\mu$ was 59%, as mentioned, and was a significant improvement on the previous value of 43.9%, which allows a stronger limit to be set. The leakage values were between 1.5% and 3.5% depending on the final state and again this improved on the old

values of 6%. Most importantly there was a substantial reduction in the variation between models. In the $\mu\mu$ channel the difference between the highest and lowest values was roughly 14%, much lower than the 29% from the previous analysis.

Table 2: Lepton cuts defining the fiducial region.

	Electron requirement	Muon requirement
Leading lepton p_T	$p_T > 25$ GeV	$p_T > 20$ GeV
Sub-leading lepton p_T	$p_T > 20$ GeV	$p_T > 20$ GeV
Lepton η	$\lvert\eta\rvert < 1.37$ or $1.52 < \lvert\eta\rvert < 2.47$	$\lvert\eta\rvert < 2.5$
Isolation	$p_T^{cone0.3}/p_T < 0.1$	$p_T^{cone0.4}/p_T < 0.06$ and $p_T^{cone0.4} < 4$ GeV $+ 0.02 \times p_T$

Using these values for ϵ_{fid} and (4.4), we calculated the set of observed limits in Table 3 - note the expected limits are the limits set with the background only hypothesis derived from our background estimates. Again these values come from [41]. A theorist can calculate the prediction of their model in the fiducial region and use these values to see if it has been excluded.

Table 3: Expected and observed limits on the cross section for same sign lepton pairs from new physics in the fiducial region.

Mass range	95% C.L. upper limit [fb]					
	expected	observed	expected	observed	expected	observed
	$e^{\pm}e^{\pm}$		$e^{\pm}\mu^{\pm}$		$\mu^{\pm}\mu^{\pm}$	
$m > 15$ GeV	$45.5^{+14.5}_{-11.5}$	41.5	$56.2^{+23.3}_{-14.5}$	64.1	$24.0^{+8.9}_{-6.0}$	29.8
$m > 100$ GeV	$24.1^{+8.9}_{-6.2}$	23.4	$23.0^{+9.1}_{-6.7}$	31.2	$12.2^{+4.5}_{-3.0}$	15.0
$m > 200$ GeV	$8.8^{+3.4}_{-2.1}$	7.5	$8.4^{+3.4}_{-1.7}$	9.8	$4.3^{+1.8}_{-1.1}$	6.7
$m > 300$ GeV	$4.5^{+1.8}_{-1.3}$	3.9	$4.1^{+1.8}_{-0.9}$	4.6	$2.4^{+0.9}_{-0.7}$	2.6
$m > 400$ GeV	$2.9^{+1.1}_{-0.8}$	2.4	$3.0^{+1.0}_{-0.8}$	3.1	$1.7^{+0.6}_{-0.5}$	1.7

4.3.6 Optimising for the DCH

In the second paper, the above model independent analysis was optimised for the specific case of the H_L and H_R from the left-right symmetric model. As we mentioned the H_L behaves identically to the ZBM k as far as this analysis is concerned. Now the cross section to same sign leptons in this model is dependent on the mass of DCH and so due to non-observation of such events in the above analysis we can put a limit on the mass of these particles.

The benefit of having the experimentalists perform a search for a specific model is that we have access to the event selection criteria and thus do not need to go through the fiducial region step. This way we do not get the same reduction in the limit that ϵ_{fid} introduces. The basic idea is that we now compare the limit on the cross section derived in small invariant mass windows with the cross section predicted by the left-right symmetric model for different masses. In this way we derived an expected and observed limit on the cross section times branching ratio, shown in Figure 4.6, and accordingly the limit on new particle masses, as in Table 4 (both taken from [42]). We have not included the limits on H_R in the table as they are not interesting for our purposes. Note that the limit obtained of course depends on the branching fraction to the different final states, which is a free parameter in the models. Nonetheless this is usually constrained by experimental limits from, for example, $\beta\beta0\nu$.

Table 4: Lower mass limits at 95% CL on H_L for different final states and branching ratios. Note that these limits are completely transferable to the ZBM k.

BR($H_L^{\pm\pm} \to \ell^\pm\ell'^\pm$)	95% CL lower limit on $m(H_L^{\pm\pm})$ [GeV]					
	$e^\pm e^\pm$		$\mu^\pm\mu^\pm$		$e^\pm\mu^\pm$	
	exp.	obs.	exp.	obs.	exp.	obs.
100%	407	409	401	398	392	375
33%	318	317	317	290	279	276
22%	274	258	282	282	250	253
11%	228	212	234	216	206	190

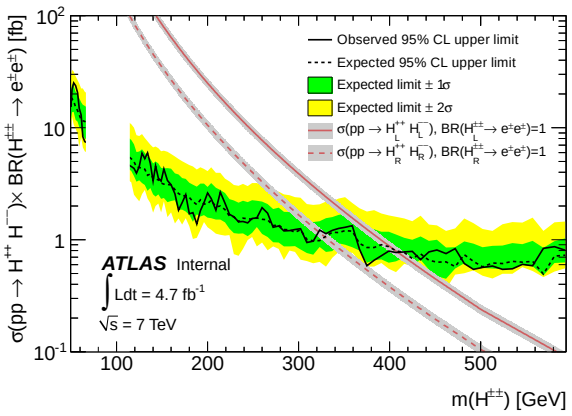

(a)

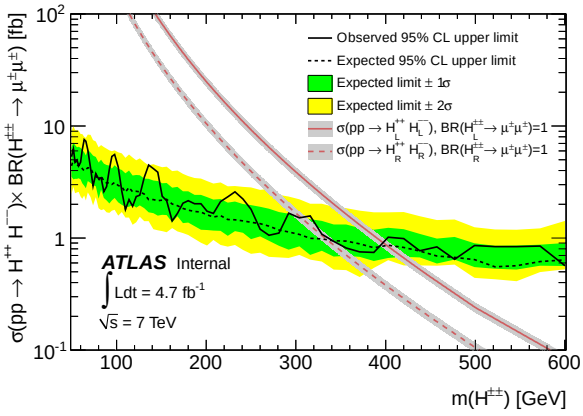

(b)

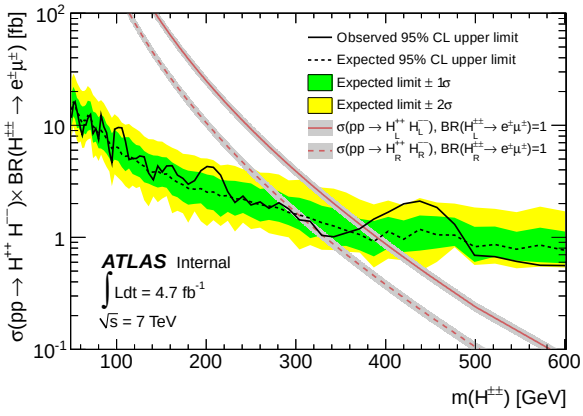

(c)

Figure 4.6: 95% CL upper limit on the cross section times branching ratio for pair production of the DCH decaying into (a) ee, (b) $\mu\mu$, and (c) $e\mu$ pairs.

5 Conclusion

The discovery at the LHC of a Higgs-like resonance at 126 GeV shows that we are on the verge of entering the regime of physics beyond the SM: the BSM era. This is the realm of famous problems such as dark matter, matter-antimatter asymmetry, unification of gauge forces or quantum gravity. Even if not as well known, there are good reasons to see the problem of neutrino mass as a preeminent BSM concern. There is direct experimental evidence that neutrinos have mass - in blatant conflict with the SM prediction - and there is already a dense forest of neutrino mass models seeking to cure this defect. Nevertheless Babu and Leung's proposal of approaching the problem from the perspective of effective operators rather than models may well provide a simple route through the landscape.

A key theme of this thesis has been contributing to the growing work on effective neutrino mass operators, which has already been considerably built on by the work of de Gouvêa and Jenkins as well as Volkas and Angel. In section 2 we took the first steps towards the goal of excluding all dimension 11 operators. Our initial aim of ruling out models from two arbitrary 11D operators was revealed to be naive. It appears that 11D operators are tightly coupled to their lower dimension counterparts and generating a model that is truly 11D in origin is more challenging than initially thought; indeed it may not even be possible and this is further work that must be investigated. In the process of analysing a model from $\mathcal{O}_{68_b}$ and $\mathcal{O}_{31_a}$, we needed to evaluate two loop integrals exactly. The details of this have been presented in appendices A and B. From appendix B we learn that two loop integrals with odd numerators need not vanish. This seems in conflict with a conclusion reached by de Gouvêa and Jenkins and may necessitate a reconsideration of their scale of new physics analysis for several operators.

In section 3 we detailed a number of constraints that exist on the pathway Volkas and Angel outlined for going from effective operators to models. The most interesting conclusion of these various restrictions is that it appears the possible models that can be realised from 9D operators is not as numerous as first expected. If 11D operators are truly ruled out, this bodes well for moving through their 9D counterparts quickly.

Finally in section 4 we outlined how the LHC can be exploited as a powerful source of constraints on neutrino mass models. We did this by analysing the Zee-Babu Model k particle and demonstrating limits on it were equivalent to limits on the left handed doubly charged Higgs from the left-right symmetric model. Through playing a part in this analysis we were able to contribute towards a mass limit on the k particle, displayed in Table 4. The high reach of such limits demonstrates that LHC data will be an important counterpart to precision data when it comes to ruling out models and thus operators.

The combination of a systematic approach to neutrino mass models with new experimental data from the LHC and upcoming precisions experiments, is a strong reason to be optimistic about the resolution of this SM shortcoming. This is an exciting realisation not just for neutrino physics, but for physics as a whole. As seen, essentially all neutrino mass models introduce new particles at higher energy scales. If we are able to figure out the one used by nature, then understanding such particles will likely act as a portal to new BSM phenomena and potentially even more discoveries.

A Techniques for Evaluating Two Loop Integrals

In this appendix we outline the details of how to calculate two loop integrals. In order to do this the notation and work of van der Bij and Veltman will be utilised [45]. This approach was motivated by its application to an exact determination of the Zee-Babu Model diagram by McDonald and McKellar [46].

The general problem contains two parts: 1. Reduce the integral to simpler integrals of the form $(2m|m_1|m_2)$ - the notation will be explained shortly; and 2. Exactly evaluate this simpler integral. There are two circumstances where this procedure can fail at stage 1. If the integral contains a mass that is repeated more than once in the same loop and this occurs for both loops (e.g. the p loop has m_1 appearing twice and the q loop has m_2 appearing twice), then the integral cannot easily be reduced. This is highly unlikely to arise in neutrino mass models and so is not discussed here further, but some details are mentioned in [45]. The other situation in which this can fail is if there is an odd numerator, e.g. $p \cdot q$ as in $\mathcal{M}^2_{ab}$ from section 2. This situation is a bit more difficult and has not been evaluated in the literature. Appendix B provides a derivation for the integral we are interested in and this should provide sufficient guidance for evaluating such integrals more generally.

Reduction to $(2m|m_1|m_2)$

The first step is to remove any terms on the numerator. Even terms can be removed through repeated use of the following trick: $p^2 = (p^2 + m^2) - m^2$. Odd terms are discussed in appendix B. Once the numerators have been removed it is convenient to utilise the following notation from [45]:

$$\begin{aligned}&(M_{11}, ..., M_{1n_1}|M_{21}, ..., M_{2n_3}|M_{31}, ..., M_{3n_3}) \\ &\equiv \int d^n p \int d^n q \prod_{i=1}^{n_1}\prod_{j=1}^{n_2}\prod_{k=1}^{n_3} \frac{1}{p^2 + M_{1i}^2}\frac{1}{p^2 + M_{1i}^2}\frac{1}{q^2 + M_{2i}^2}\frac{1}{(p+q)^2 + M_{3i}^2},\end{aligned} \tag{A.1}$$

where n is used rather than 4 as we will evaluate the divergences in the integral using dimensional regularization. Now we can see that $(2m|m_1|m_2)$ is just a two loop integral, where the $2m$ is shorthand for m, m.

Once we have the integral in the form of (A.1) there are two steps to reduce it to the desired form. Firstly we reduce the integral to terms of the form $(m|m_1|m_2)$ through repeated use of the following expression and its obvious generalisations:

$$(m, m_0|m_1|m_2) = \frac{1}{m^2 - m_0^2}\left[(m_0|m_1|m_2) - (m|m_1|m_2)\right], \tag{A.2}$$

which is just partial fractions. Secondly we turn these integrals into the desired form using:

$$(m_0|m_1|m_2) = -\left[m_0^2\,(2m_0|m_1|m_2) + m_1^2\,(2m_1|m_0|m_2) + m_2^2\,(2m_2|m_0|m_1)\right], \tag{A.3}$$

which can be proven using 't Hooft's partial p formula [47]. Now the problem has been reduced to evaluating $(2m|m_1|m_2)$.

Determination of $(2m|m_1|m_2)$

To begin with recall:

$$(2m|m_1|m_2) \equiv \int d^n p \int d^n q \frac{1}{\left(p^2+m^2\right)^2} \frac{1}{\left(q^2+m_1^2\right)} \frac{1}{\left(\left[p+q\right]^2+m_2^2\right)} \tag{A.4}$$

This integral has been exactly evaluated in the literature. Unfortunately there is some disagreement in the result, compare [45] and [46]. In order to determine which to use key parts of the calculation were repeated. Even though this may appear a relatively simple two loop integral, the calculation is quite in depth and we just provide a rough outline of the steps involved here. The first step is to perform the p and q integrations. This can be done with the following four expressions:

$$\begin{array}{c} \frac{1}{a^\alpha b^\beta} = \frac{\Gamma(\alpha+\beta)}{\Gamma(\alpha)\Gamma(\beta)} \int_0^1 dx \frac{x^{\alpha-1}(1-x)^{\beta-1}}{(ax+b[1-x])^{\alpha+\beta}} \\ \int d^n t \frac{1}{t^2+m^2} = i\pi^{n/2} \frac{\Gamma(2-n/2)}{\Gamma(2)} \frac{1}{\left(m^2\right)^{2-n/2}} \\ \int d^n p \frac{p^2}{\left(p^2+m^2\right)^{5-n/2}} = i\pi^{n/2} \frac{n}{2} \frac{\Gamma(4-n)}{\Gamma(5-n/2)} \frac{1}{\left(m^2\right)^{4-n}} \\ \int d^n p \frac{1}{\left(p^2+m^2\right)^{5-n/2}} = i\pi^{n/2} \frac{n}{2} \frac{\Gamma(5-n)}{\Gamma(5-n/2)} \frac{1}{\left(m^2\right)^{5-n}}, \end{array} \tag{A.5}$$

where Γ is the gamma function. The first expression here is just the generalised Feynman parameter formula [48] and the last three are standard integrals [47]. After using these and a bit of algebra we conclude

$$\begin{array}{c} (2m|m_1|m_2) = \frac{-\pi^4\left(\pi m^2\right)^{n-4}\Gamma(2-n/2)}{\Gamma(3-n/2)} \int_0^1 dx \int_0^1 \left[x\left(1-x\right)\right]^{n/2-2} y\left(1-y\right)^{2-n/2} \\ \times \left[\Gamma\left(5-n\right) \frac{\mu^2}{\left(y+\mu^2(1-y)\right)^{5-n}} + \frac{n}{2}\Gamma\left(4-n\right) \frac{1}{\left(y+\mu^2(1-y)\right)^{4-n}}\right], \end{array} \tag{A.6}$$

where the x and y integrals originate from using the Feynman parameter expression twice and μ^2 is a simplifying expression introduced, defined by

$$\mu^2 \equiv \frac{ax+b\left(1-x\right)}{x\left(1-x\right)}, \quad a \equiv \frac{m_1^2}{m^2}, \quad b \equiv \frac{m_2^2}{m^2} \tag{A.7}$$

(A.6) should make it apparent why it was necessary to evaluate the integrals in nD rather than 4D - naively setting $n = 4$ gives expressions like $\Gamma\left(0\right)$, which diverge. This suggests $(2m|m_1|m_2)$ contains divergent terms, but this should have been expected: there is only a single q propagator and standard cutoff regularizing shows such integrals should be log divergent. What should be convergent is the total contribution of all these integrals and confirming all the divergent terms cancel is a good cross check against algebraic mistakes.

In order to simplify (A.6) we set $n = 4 + \epsilon$ and keep only term less than $\mathcal{O}\left(\epsilon\right)$ as when we eventually take $\epsilon \to 0$ such terms vanish. Then we use the following two asymptotic expressions

$$[f(x)]^{\epsilon} = 1 + \epsilon \log[f(x)] + \tfrac{1}{2}(\log[\epsilon f(x)])^2 + \mathcal{O}(\epsilon^3)$$
$$\Gamma(\epsilon) = \tfrac{1}{\epsilon} - \gamma_E + \epsilon\left(\tfrac{1}{12}\pi^2 + \tfrac{1}{2}\gamma_E^2\right) + \mathcal{O}(\epsilon^2), \tag{A.8}$$

where γ_E is the Euler-Mascheroni constant. Using these one can break up (A.6) into separate integrals that can be evaluated, taking care to ensure all terms of order less than ϵ are retained when everything is brought back together. Although this involves a lot of algebra, by the usual miracle of Feynman diagram calculations this eventually simplifies to give

$$\begin{aligned}(2m|m_1|m_2) &= \pi^4\left[-\tfrac{2}{\epsilon^2} + \tfrac{1}{\epsilon}(1 - 2\gamma_E - 2\log[\pi m^2])\right] \\ +\pi^4\left[-\tfrac{1}{2} - \tfrac{1}{12}\pi^2 + \gamma_E - \gamma_E^2 + (1-2\gamma_E)\log[\pi m^2] - \log^2[\pi m^2] - f(a,b)\right] &+ \mathcal{O}(\epsilon),\end{aligned} \tag{A.9}$$

where we have defined

$$f(a,b) = \int_0^1 dx \left[\mathrm{Li}_2\left(1-\mu^2\right) - \frac{\mu^2 \log \mu^2}{1-\mu^2}\right] \tag{A.10}$$

and Li_2 is the dilogarithm function defined by:

$$\mathrm{Li}_2(x) \equiv \int_0^x \frac{\log[1-y]}{y} dy \tag{A.11}$$

The evaluation of $f(a,b)$ requires further work, but before doing this it is worth pointing out what (A.9) tells us. As alluded to above we can now explicitly see that $(2m|m_1|m_2)$ is a divergent integral and the divergence is not simply constant, but rather depends on m also. The convergence of the integral cannot depend on certain choices of the masses and so the divergences must cancel between terms with the same masses in the p integral. We can then just treat all terms in (A.9) - except for f, which depends on all the masses - as a function of m, say $g(m) \neq 0$. Then the convergence of the integral ensures not only the divergent terms cancel, but that everything in (A.9) except for f cancels. This makes sense as many of these terms are proportional to γ_E, which is a relic of our choice of regularization technique and so the physical part of the integral should not depend on it.

Accordingly once we have ensured our model is convergent, taking $\epsilon \to 0$ is equivalent to treating the integral using the following 'effective' expression:

$$(2m|m_1|m_2)_{Eff} \equiv -\pi^4 f(a,b) \tag{A.12}$$

(A.12) is deceptively simple, there is still a lot of work to do to put f in a form that we can put into Mathematica. After calculating the integrals, one can finally show that

$$\begin{aligned}(2m|m_1|m_2)_{Eff} &= \tfrac{\pi^4}{2}\log a \log b \\ +\tfrac{\pi^4}{2}\left(\tfrac{a+b-1}{c}\right)&\left[\mathrm{Li}_2\left(\tfrac{-x_2}{y_1}\right) + \mathrm{Li}_2\left(\tfrac{-y_2}{x_1}\right) - \mathrm{Li}_2\left(\tfrac{-x_1}{y_2}\right) - \mathrm{Li}_2\left(\tfrac{-y_1}{x_2}\right)\right. \\ &\left. + \mathrm{Li}_2\left(\tfrac{b-a}{x_2}\right) + \mathrm{Li}_2\left(\tfrac{a-b}{y_2}\right) - \mathrm{Li}_2\left(\tfrac{b-a}{x_1}\right) - \mathrm{Li}_2\left(\tfrac{a-b}{y_1}\right)\right],\end{aligned} \tag{A.13}$$

where a and b are as in (A.7) and c, $x_{1,2}$ and $y_{1,2}$ are defined by:

$$\begin{aligned} c &\equiv \sqrt{1-2\left(a+b\right)+\left(a-b\right)^2} \\ x_{1,2} &\equiv \left(1+b-a\pm c\right)/2 \\ y_{1,2} &\equiv \left(1+a-b\pm c\right)/2 \end{aligned} \tag{A.14}$$

There are actually a number of different ways that (A.13) can be written - see [45], where approximate expressions for the integral in different mass limits is also provided. The form written, however, is the most useful for computing values in Mathematica as other expressions involve logarithms that will give imaginary answers without a judicious branch choice. Accordingly we now have an exact expression for $(2m|m_1|m_2)$ as desired.

B Evaluating $p \cdot q$ Type Two Loop Integrals

In appendix A we saw how to evaluate two loop integrals when the numerator is even. The problem involving odd numerators has been considered in the literature, but only in the case of finite external momenta [49]. This case is relevant if one is, for example, considering the second order Higgs correction to the ρ-parameter [45]. For a neutrino mass, however, we want the rest mass and so need the zero external momenta case. One cannot simply take a limit between the two as the expressions are typically divergent in this limit.

Accordingly we here present the details of how to evaluate the $p \cdot q$ integral that appeared in section 2.1.2, where it was called I_{cd}^{2B}. This should provide sufficient detail to evaluate such integrals in general. To begin with we want to get rid of the numerator which we can do using:

$$p \cdot q = \frac{1}{2}\left[\left(p+q\right)^2+m^2\right] - \frac{1}{2}p^2 - \frac{1}{2}q^2 - \frac{1}{2}m^2 \tag{B.1}$$

This means we will break the integral into four separate integrals. The integral with the p^2 term in the numerator can simply be merged with I_{cd}^{2A}, which we already independently checked to be convergent. Thus the remaining terms must be convergent amongst themselves. Using $q^2 = (q^2+m_{S2}^2) - m_{S2}^2$ and the notation from appendix A, the remaining terms in I_{cd}^{2B} reduce to:

$$\begin{aligned} &\tfrac{1}{2}\left(m_c, m_{F1}, m_{S1}|m_{S3}|m_d\right) + \tfrac{1}{2H}\left(m_c, m_{F1}, m_{S1}|m_{S2}, m_{S3}|m_d\right) \\ &\quad -\tfrac{1}{2}\left(d^n p \tfrac{1}{p^2+m_c^2}\tfrac{1}{p^2+m_{F1}^2}\tfrac{1}{p^2+m_{S1}^2}\right)\left(d^n q \tfrac{1}{q^2+m_{S2}^2}\tfrac{1}{q^2+m_{S3}^2}\right) \end{aligned} \tag{B.2}$$

where $H = (m_d^2 - m_{S2}^2)^{-1}$. Using appendix A we know how to calculate the two loop integrals in the first line. The problem is the expression in the second line, which is a product of decoupled one loop integrals. Naively this appears simple, as one loop integrals are much better understood than two loop integrals. Nevertheless the problem is that when taking the product of two one loop integrals, terms of $\mathcal{O}\left(\epsilon^{-1}\right)$ on one side can combine with terms $\mathcal{O}\left(\epsilon\right)$ on the other to give convergent contributions and one loop integrals are not usually evaluated up to this order.

The one loop integrals in (B.2) can be reduced to several integrals of a single denominator using partial fractions. Then using standard techniques for calculating divergent one loop integrals, see e.g. [50], one can show:

$$\int d^{4+\epsilon}t \frac{1}{t^2-m^2} = -i\pi^2 m^2 \left(\pi m^2\right)^{\epsilon/2} \Gamma\left(-1-\epsilon/2\right) \tag{B.3}$$

Next we can use the following expansions for small ϵ:

$$\begin{array}{c} \left(\pi m^2\right)^{\epsilon/2} = 1 + \frac{\epsilon}{2}\log\left(\pi m^2\right) + \frac{\epsilon^2}{8}\log^2\left(\pi m^2\right) + \mathcal{O}\left(\epsilon^3\right) \\ \Gamma\left(-1-\epsilon/2\right) = \frac{2}{\epsilon} - \psi\left(2\right) + \frac{\epsilon}{4}\left(\frac{\pi^2}{3} + \psi^2\left(2\right) - \psi'\left(2\right)\right) + \mathcal{O}\left(\epsilon^2\right), \end{array} \tag{B.4}$$

where ψ is the Euler Digamma function, in particular $\psi\left(2\right) = 1-\gamma_E$ and $\psi'\left(2\right) = \pi^2/6 - 1$. Accordingly we have:

$$\int d^{4+\epsilon}t \frac{1}{t^2-m^2} = i\pi^2 m^2 \left[-\frac{2}{\epsilon} + \gamma_m - \frac{\epsilon}{4}\left(\frac{\pi^2}{6} + 1 + \gamma_m^2\right)\right] + \mathcal{O}\left(\epsilon^2\right), \tag{B.5}$$

where we have defined $\gamma_m \equiv 1 - \gamma_E - \log\left(\pi m^2\right)$. From here one can show the second line of (B.2) can be evaluated as:

$$\begin{array}{c} \frac{\pi^4}{\epsilon}\left[DGm_{S1}^2\gamma_{m_{S1}} - DEm_{F1}^2\gamma_{m_{F1}} + EGm_c^2\gamma_{m_c}\right] \\ +\pi^4\left[\frac{1}{4}\left(DEm_{F1}^2\gamma_{m_{F1}}^2 - EGm_c^2\gamma_{m_c}^2 - DGm_{S1}^2\gamma_{m_{S1}}^2\right) + \frac{1}{2}\left(m_{S3}^2\gamma_{m_{S3}} - m_{S2}^2\gamma_{m_{S2}}\right)\right. \\ \left.\times\left(ADGm_{S1}^2\gamma_{m_{S1}} - ADEm_{F1}^2\gamma_{m_{F1}} + AEGm_c^2\gamma_{m_c}\right)\right] + \mathcal{O}\left(\epsilon\right), \end{array} \tag{B.6}$$

where $A = \left(m_{S2}^2 - m_{S3}^2\right)^{-1}$, $D = \left(m_{F1}^2 - m_{S1}^2\right)^{-1}$, $E = \left(m_c^2 - m_{F1}^2\right)^{-1}$ and $G = \left(m_c^2 - m_{S1}^2\right)^{-1}$. Carefully combining this with the two loop integrals provides a convergent result and we find that (B.2) evaluates to:

$$\begin{array}{c} \frac{1}{2}\left[\pi^4 ADEG\left\{m_{F1}^2 m_{S1}^2 \log\left(\frac{m_{S1}^2}{m_{F1}^2}\right)\left[m_{S2}^2\log\left(\pi m_{S2}^2\right) - m_{S3}^2\log\left(\pi m_{S3}^2\right)\right]\right.\right. \\ +m_c^2 m_{F1}^2 \log\left(\frac{m_{F1}^2}{m_c^2}\right)\left[m_{S2}^2\log\left(\pi m_{S2}^2\right) - m_{S3}^2\log\left(\pi m_{S3}^2\right)\right] \\ \left.+m_{S1}^2 m_c^2 \log\left(\frac{m_c^2}{m_{S1}^2}\right)\left[m_{S2}^2\log\left(\pi m_{S2}^2\right) - m_{S3}^2\log\left(\pi m_{S3}^2\right)\right]\right\} \\ +m_{S1}^2 ADG\left\{\frac{1}{H}\left(2m_{S1}|m_{S2}|m_d\right) - \frac{1}{I}\left(2m_{S1}|m_{S3}|m_d\right)\right\} \\ -m_{F1}^2 ADE\left\{\frac{1}{H}\left(2m_{F1}|m_{S2}|m_d\right) - \frac{1}{I}\left(2m_{F1}|m_{S3}|m_d\right)\right\} \\ +m_c^2 AEG\left\{\frac{1}{H}\left(2m_c|m_{S2}|m_d\right) - \frac{1}{I}\left(2m_c|m_{S3}|m_d\right)\right\} \\ +m_{S3}^2\frac{A}{2I}\left\{DG\left(2m_{S3}|m_{S1}|m_d\right) - DE\left(2m_{S3}|m_{F1}|m_d\right) + EG\left(2m_{S3}|m_c|m_d\right)\right\} \\ +m_{S2}^2\frac{A}{2H}\left\{-DG\left(2m_{S2}|m_{S1}|m_d\right) + DE\left(2m_{S2}|m_{F1}|m_d\right) - EG\left(2m_{S2}|m_c|m_d\right)\right\} \\ +m_d^2\frac{A}{2I}\left\{DG\left(2m_d|m_{S1}|m_{S3}\right) - DE\left(2m_d|m_{F1}|m_{S3}\right) + EG\left(2m_d|m_c|m_{S3}\right)\right\} \\ \left.+m_d^2\frac{A}{2H}\left\{-DG\left(2m_d|m_{S1}|m_{S2}\right) + DE\left(2m_d|m_{F1}|m_{S2}\right) - EG\left(2m_d|m_c|m_{S2}\right)\right\}\right] \end{array} \tag{B.7}$$

where $I = \left(m_d^2 - m_{S3}^2\right)^{-1}$ and as this is convergent, all terms of the form $\left(2m|m_1|m_2\right)$ should be replaced with their 'effective' part as defined in appendix A. One feature of this expression that may appear unusual is the presence of a dimensionful argument in the logarithms. The correct way to remove this is to make all couplings dimensionless, and then the masses removed from the couplings combine with the arguments to form dimensionless quantities, see e.g. [51]. Nonetheless the result obtained is numerically identical and so was not calculated.

C Time-symmetric Quantization and Hawking Radiation

In addition to the above work, the author also collaborated with Dr Kobakhidze on a project where we were able to show that the standard time-asymmetric quantization of fields in QFT is a necessary condition to the existence of Hawking Radiation [52]. We did this by demonstrating that in a theory with a time-symmetric quantization, Unruh radiation - a conceptual precursor to the Hawking effect - does not arise. This work was motivated by the fact that while Hawking radiation has a number of attractive features, such as the suggestive consistency it provides to Bekenstein's black hole entropy, it also leads to a number of theoretical problems. These include the famous black hole information loss paradox, which arises from the loss of unitarity at the horizon. Accordingly we were interested in seeing whether a consistent framework could be constructed without Hawking radiation and thereby determining what are the necessary conditions in the canonical approach that give rise to this effect.

Unfortunately there is not space here to provide all the details but the basics are as follows. We considered the problem from the simplified perspective of a free massless scalar field and quantised it as follows:

$$\hat{\phi}(t,x) = \int dk \left(f_k \hat{A}_k + f_k^* \hat{A}_k^\dagger \right) \ , \tag{C.1}$$

where $f_k = \frac{1}{2\pi\sqrt{2|k|}} \mathrm{e}^{-i(|k|t-kx)}$ and instead of the standard $\hat{A}_k = \hat{a}_k$, we take

$$\hat{A}_k = \frac{1}{\sqrt{2}} \left(\hat{a}_k + \hat{\alpha}_{-k}^\dagger \right) \ , \ \left[\hat{A}_k^\dagger \equiv (\hat{A}_k)^\dagger \right] \ . \tag{C.2}$$

This choice implies a manifest time symmetry of $t \to -t$ in $\hat{\phi}(t,x)$ as opposed to the standard anti-unitary transformation. One can then show the creation $\hat{a}_k^\dagger$, $\hat{\alpha}_k^\dagger$ and annihilation $\hat{a}_k$, $\hat{\alpha}_k$ operators obey the following relations:

$$[\hat{a}_k, \hat{a}_{k'}^\dagger] = 2\pi\delta(k-k'), \ \ [\hat{\alpha}_k, \hat{\alpha}_{k'}^\dagger] = -2\pi\delta(k-k') \tag{C.3}$$

Furthermore one can then calculate all basic features of the free field theory and demonstrate that this is a consistent and causal approach. The key point, however, is that when one calculates the Minkowski vacuum expectation value of the particle number operator for an accelerated observer ($\hat{N}_R$), we find:

$$\langle 0_M | \hat{N}_R | 0_M \rangle = 0, \tag{C.4}$$

instead of the traditional thermal term famous from the Unruh effect. When one goes through the calculation in detail, it turns out that the normal thermal term is exactly cancelled by an opposite sign term from the $\hat{\alpha}$ and $\hat{\alpha}^\dagger$ operators. The sign difference originates from the negative in the second commutator of (C.3).

References

[1] Y. Fukuda et al, Phys. Rev. Lett. **81** (1998) 1158.

[2] Y. Fukuda et al, Phys. Rev. Lett. **81** (1998) 1562.

[3] A. Habig, Nucl. Phys. Proc. Suppl. **218** (2011) 320.

[4] K. Babu and C. Leung, Nucl. Phys. B **619** (2001) 667.

[5] A. de Gouvêa and J. Jenkins, Phys. Rev. D **77** (2008) 013008.

[6] P. Angel and R. Volkas (supervisor), "Radiative generation of neutrino mass and lepton number violating effective operators," (MSc Thesis, Melbourne University, 2011).

[7] J. Schechter and J. Valle, Phys. Rev. D **25** (1982) 2951.

[8] J. Nieves, Phys. Lett. B **147** (1984) 375.

[9] P. Minkowski, Phys. Lett. B **67** (1977) 421.

[10] T. Yanagida, Conf. Proc. **C7902131** (1979) 95.

[11] M. Gell-Mann, P. Ramond and R. Slansky, Conf. Proc. **C790927** (1979) 315.

[12] R. Mohapatra and G Senjanovic, Phys. Lett. **44** (1980) 912.

[13] J. Pati and A. Salam, Phys. Rev. D **10** (1974) 275.

[14] R. Mohapatra and J. Pati, Phys. Rev. D **11** (1975) 566.

[15] G. Senjanovic and R. Mohapatra, Phys. Rev. D **12** (1975) 1502.

[16] T. Rizzo, Phys. Rev. D **25** (1982) 1355.

[17] H. Georgi and D. Nanopoulos, Nucl. Phys. B **159** (1979) 16.

[18] M. Magg and C. Wetterich, Phys. Lett. B **94** (1980) 61.

[19] J. Schechter and J. Valle, Phys. Rev. D **22** (1980) 2227.

[20] C. Wetterich, Nucl. Phys. B **187** (1981) 343.

[21] G. Lazarides, Q. Shafi and C. Wetterich, Nucl. Phys. B **181** (1981) 287.

[22] R. Mohapatra and G. Senjanovic, Phys. Rev. D **23** (1981) 165.

[23] T. Cheng and L. Li, Phys. Rev. D **22** (1980) 2860.

[24] R. Foot et al, Z. Phys. C **44** (1989) 441.

[25] S. Weinberg, Phys. Rev. Lett. **43** (1979) 1566.

[26] A. Zee, Nucl. Phys. B **264** (1986) 99.

[27] K. Babu, Phys. Lett. B **203** (1988) 132.

[28] ATLAS Collaboration, Phys. Rev. D **83** (2011) 112006.

[29] M. Nebot et al, Phys. Rev. D **77** (2008) 093013.

[30] The CMS Collaboration, Phys. Lett. B **716** (2012) 30.

[31] The ATLAS Collaboration, Phys. Lett. B **716** (2012) 1.

[32] The ATLAS Collaboration, The ATLAS Detector, cern.ch, at 26 September 2012.

[33] K. Babu and C. Macesanu, Phys. Rev. D **67** (2003) 073010.

[34] D. Sierra and M. Hirsch, JHEP **12** (2006) 052.

[35] The MEG Collaboration, Phys. Rev. Lett. **107** (2011) 171801.

[36] H. Georgi and M. Machacek, Nucl. Phys. B **262** (1985) 463.

[37] N. Arkani-Hamed et al, JHEP **0208** (2002) 021.

[38] P. Frampton, P. Hung and M. Sher, Phys. Rept. **330** (2000) 263.

[39] R. Barnett, J. Gunion and H. Haber, Phys. Lett. B **315** (1993) 349.

[40] J. Alwall, P. Schuster and N. Toro, Phys. Rev. D **79** (2009) 075020.

[41] The ATLAS Collaboration, arXiv:1210.4538 (submitted to JHEP), 2012.

[42] The ATLAS Collaboration, "Search for doubly charged Higgs bosons in like-sign dilepton final states with the ATLAS detector" (submitted to Eur. Phys. J. C), 2012.

[43] The ATLAS Collaboration, Phys. Rev. D **85** (2012) 032004.

[44] A. Read, J. Phys. G **28** (2002) 2693.

[45] J. van der Bij and M. Veltman, Nucl. Phys. B **231** (1984) 205.

[46] K. McDonald and B. McKellar, hep-ph/0309270.

[47] G. 't Hooft and M. Veltman, Nucl. Phys. B **44** (1972) 189.

[48] A. Ghinculov and J. van der Bij, Nucl. Phys. B **436** (1995) 30.

[49] A. Ghinculov and Y. Yao, Nucl. Phys. B **516** (1998) 385.

[50] M. Peskin and D. Schroeder, *An Introduction to Quantum Field Theory* (1995).

[51] H. Kleinert and V. Schulte-Frohlinde, *Critical Properties of ϕ^4 Theories* (2001).

[52] A. Kobakhidze and N. Rodd, "Time-symmetric quantization in spacetimes with event horizons" (submitted to IJTP), 2012.